

University of Groningen

Donor-Acceptor Stenhouse Adducts

Lerch, Michael Markus

IMPORTANT NOTE: You are advised to consult the publisher's version (publisher's PDF) if you wish to cite from it. Please check the document version below.

Document Version

Publisher's PDF, also known as Version of record

Publication date:

2018

[Link to publication in University of Groningen/UMCG research database](#)

Citation for published version (APA):

Lerch, M. M. (2018). *Donor-Acceptor Stenhouse Adducts*. Rijksuniversiteit Groningen.

Copyright

Other than for strictly personal use, it is not permitted to download or to forward/distribute the text or part of it without the consent of the author(s) and/or copyright holder(s), unless the work is under an open content license (like Creative Commons).

The publication may also be distributed here under the terms of Article 25fa of the Dutch Copyright Act, indicated by the "Taverne" license. More information can be found on the University of Groningen website: <https://www.rug.nl/library/open-access/self-archiving-pure/taverne-amendment>.

Take-down policy

If you believe that this document breaches copyright please contact us providing details, and we will remove access to the work immediately and investigate your claim.

Downloaded from the University of Groningen/UMCG research database (Pure): <http://www.rug.nl/research/portal>. For technical reasons the number of authors shown on this cover page is limited to 10 maximum.

1



“Furfurol färbt die Haut stark gelb; berührt man dann den damit gefärbten Theil mit einigen Tropfen Anilin, so verändert sich die Farbe langsam in’s Rosenrothe. Dieselbe Erscheinung zeigt sich beim Behandeln von Papier, weißer Seide, Leinwand oder Baumwollenzeug in der eben angegebenen Weise. Die rothe Färbung kommt immer erst nach einigen Minuten zum Vorschein, erhält sich dann einige Tage und geht später in’s Braungelbe über.”

Translation:

Furfural stains skin strongly yellow; once one touches the stained part with a few drops of aniline, the color changes slowly to roseate. The same phenomenon is observed for the treatment of paper, white velvet, canvas or cotton fabric when processed according to the same procedure. The red staining appears always only after a few minutes and resides for a few days before it changes into a brownish-yellow color.

Dr. J. Stenhouse, Lecture for the Royal Society of London, 18. April 1850
Justus Liebigs Ann. Chem., **1850**, 74 (3), 278–297

Chapter 1

The (Photo)chemistry of Stenhouse Photoswitches: Guiding Principles and System Design

1

Published as:

Chem. Soc. Rev., **2018**, *47*, 1910-1937

DOI: [10.1039/c7cs00772h](https://doi.org/10.1039/c7cs00772h)

Michael M. Lerch, Wiktor Szymański* and Ben L. Feringa*

ABSTRACT: *Molecular photoswitches comprise chromophores that can be interconverted reversibly with light between two states with different photochemical and physicochemical properties. This feature renders them useful for diverse applications, ranging from material science, biology (specifically photopharmacology) to supramolecular chemistry. With new and more challenging systems to control, especially extending towards biomedical applications, using visible or near-infrared light for photoswitch activation becomes vital. Donor–acceptor Stenhouse adducts are a novel class of visible light-responsive negative photochromes that provide a possible answer to current limitations of other photoswitch classes in the visible and NIR window. Their rapid development since their discovery in 2014, together with first successful examples of applications, demonstrate both their potential and areas where improvements are needed. A better understanding of DASA characteristics and its photoswitching mechanism has revealed that they are in fact a subset of a more general structural class of photochromes, namely Stenhouse photoswitches. This chapter provides an introduction and practical guide on DASAs: it focuses on their structure and synthesis, provides fundamental insights for understanding their photoswitching behavior and demonstrates guiding principles for tailoring these switches for given applications.*

1.1 Introduction

1.1.1 Molecular photoswitches

Molecular photoswitches¹ are small molecules that respond to light as an external stimulus. Upon photoswitching, the molecule undergoes a reversible change in geometry, polarity and charge distribution.² Most common photoswitches include azobenzenes, stilbenes, spiropyrans/spirooxazines, diarylethenes, hemithioindigo photoswitches, fulgides, fulgimides and acylhydrazones. They operate through either a *trans–cis* double-bond photoisomerization (azobenzenes, stilbenes, acylhydrazones and hemithioindigo photoswitches) or a light-activated cyclization/ring-opening reaction (diarylethenes, spiropyrans/spirooxazines and fulgides/fulgimides). Depending on the height of the energetic barrier between the two states, and the photoswitching mechanism, a photoswitch can be bistable (P-type, e.g. diarylethenes) or thermally reversible (T-type, e.g. spiropyrans). Bi-directional switching employing two different wavelengths of light relies on a change in the absorption spectrum upon photoswitching together with appropriate thermal stabilities of the isomers.

The basis for photoswitching is light absorption. Light as an external stimulus offers powerful advantages over other stimuli (e.g. pH, small molecules, mechanical force or temperature): it does not contaminate the studied sample or system, is orthogonal to most processes, is non-toxic and can be delivered in a non-invasive manner. Moreover, the instrumentation for light-delivery has rapidly developed in recent decades – especially in the medical realm – which now allows for the delivering of light with high spatial and temporal precision with the intensity and wavelength desired.

What sets photoswitches apart from other light-mediated molecular tools³ is their reversibility. In contrast to the irreversible removal of photolabile protecting groups (uncaging),⁴ photoswitches can be switched back and forth, usually with little fatigue (decomposition). While for many applications irreversible manipulation will suffice, living systems and more complex materials benefit from reversible interventions. Therefore, photoswitches have had a profound impact on fields such as material sciences, supramolecular chemistry, chemical biology, surface chemistry, catalysis and recently even medical applications (photopharmacology).⁵⁻⁷ Every photoswitch has its specific set of properties that can be tuned and need to be taken into account when a photoswitch is chosen for a given application. These include high quantum yields (ϕ), high extinction coefficients (ϵ) at visible to near-infrared (NIR) wavelengths, spectral shape, high photostationary states (PSS), control over switching speed, tunable thermal stability of the isomers and resistance against photodegradation (fatigue). Such tuning of photoswitch properties requires a thorough understanding of structure-property relationships and the photoswitching mechanism. The definition of what constitutes an ideal photoswitch depends on the application. Therefore, the researcher has to match system/application and photoswitch by focusing on one or more of the most desired properties.

1.1.2 Towards visible and NIR photoswitching

Light carries energy that is used for the switching process. Visible and NIR-activation of photoswitches has received increasing attention primarily because energy-rich UV-light can cause photodamage in biological samples and shows reduced tissue penetration.⁸⁻¹⁰ Conversely, the use of red-shifted and thus less energy-rich light limits the set of photochemical transformations available and poses a challenge to the synthetic photochemist.¹⁰ Red-shifting can come with pay-offs at other characteristics, such as synthetic accessibility, solubility, molecular size and long half-life of the thermally unstable isomer.

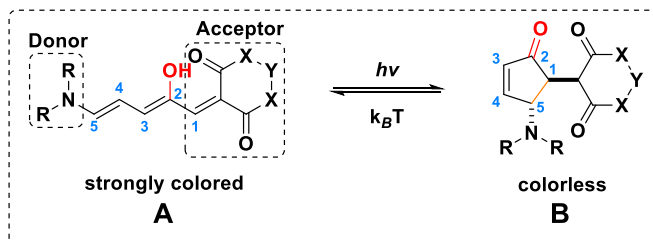
A common problem for photoswitching – particularly at high concentrations and high extinction coefficients – is that most of the light is absorbed within the outermost layer of the sample. Negative (reverse) photochromism¹¹ overcomes this limitation, as the stable form, which is usually strongly colored, undergoes photobleaching upon photoswitching to a thermally unstable, colorless state.² As the photoisomerization proceeds, photoswitching at greater depth of the sample becomes easier because of a lack of the colored form and hence light absorption.

1.1.3 Donor–acceptor Stenhouse adducts

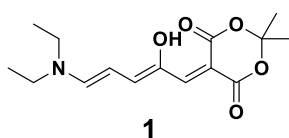
In 2014, Read de Alaniz and co-workers described the photochromism of a new class of negatively photochromic photoswitches (Figure 1.1, compound **1**, first-generation), which they termed donor–acceptor Stenhouse adducts (DASAs) in recognition of the late John Stenhouse (1809-1880).^{12,13} In 2016, first-generation DASAs were complemented with a second-generation (Figure 1.1, compound **2**).^{14,15} DASAs naturally absorb visible light and their synthesis is modular, making use of the inexpensive (bio-based) feedstock chemical furfural.

Upon irradiation of the strongly colored elongated triene form (A), rapid photobleaching leads to a colorless cyclopentenone (B). This large structural change upon photoswitching holds great promise for possible applications, some of which have already been explored in the past three years.

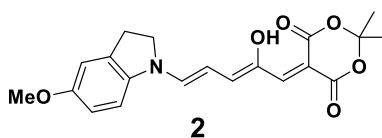
Donor–Acceptor Stenhouse Adducts (DASAs)



Meldrum's acid: $X = O, Y = C(Me)_2$
 1,3-dimethyl barbituric acid: $X = NMe, Y = C=O$



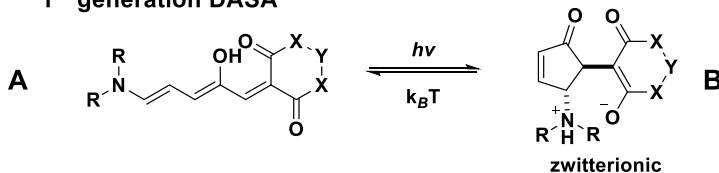
1st generation



2nd generation



1st generation DASA



2nd generation DASA

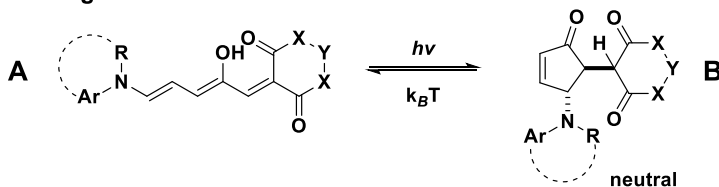


Figure 1.1 | Structure and photoswitching of donor–acceptor Stenhouse adducts.

1.2 Synthesis

In DASAs, a donor moiety is connected to an acceptor (either Meldrum's acid **3** or 1,3-dimethyl barbituric acid **4**) through a triene ("polymethine") bridge, which makes DASA a push-pull system. This modular build-up not only is a key feature governing most of DASA photochemistry, but is also a guiding principle for their synthesis (Figure 1.2).^{12,13} The triene bridge is based on furfural (**5**) and the furan oxygen is responsible for the formation of the hydroxy group (C₂-position).

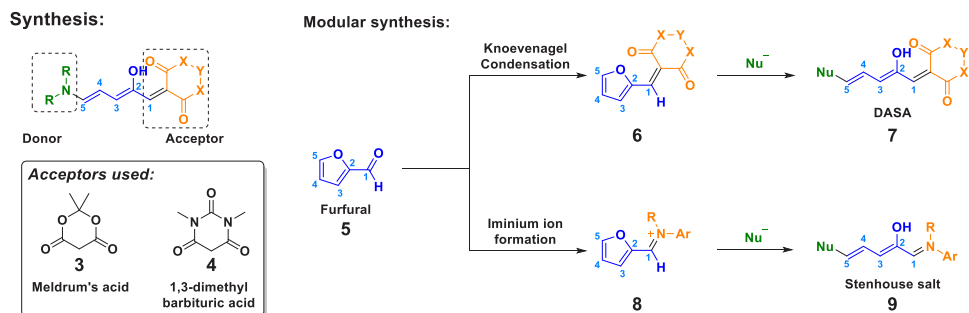


Figure 1.2 | Synthesis of DASAs and Stenhouse salts.

In the standard synthetic route, the acceptor is initially fused to furfural (**5**) by means of a Knoevenagel condensation to yield **6**. The activated furan core is subsequently opened with a nitrogen nucleophile (the donor) through a series of rearrangements around the furan core reminiscent of the (aza-)Piancatelli rearrangement^{13,16,17} resulting in the final DASA compound **7**. Stenhouse salts, which have first been described by John Stenhouse in 1850,¹⁸ make use of a formation of an iminium species/Schiff base to yield **8**. Ring-opening with a nucleophile, which is usually the same as that was used for activation, results in Stenhouse salt **9**. Formation of Stenhouse salts relies on acid addition.

The proposed mechanism of the (aza-)Piancatelli reaction gives insights into the ring-opening reaction and formation of both DASAs and Stenhouse salts (Figure 1.3).^{13,16,17} 2-Furylcarbinol (**10**) rearranges in an acidic environment through a cascade (intermediates **i** to **v**) to form *trans*-di-substituted cyclopentenone **11**. The "unfolded" intermediate **iii** corresponds to **A**, whereas **11** corresponds to **B**. Notably, in the (aza-)Piancatelli reaction, the cascade proceeds to **11** without stopping at **iii**. The condensation reaction activates the furan core for nucleophilic attack, presumably by increasing the electrophilicity of the position to be attacked and allowing a resonance structure similar to **i**. Most commonly employed acceptors for activation are Meldrum's acid (**3**) and 1,3-disubstituted barbituric acid (**4**). The ring-opening reaction strongly depends on electronics of the furan core and sterics and nucleophilicity of the nucleophile. In general, Meldrum's acid derivatives are more easily opened as compared to 1,3-dimethyl barbituric acid derivatives.¹⁹ The presence of Lewis acids might help to further activate the furan core for ring-opening.¹⁷ Notably, reaction conditions for the ring-opening step should not be completely dry.

The (Aza-)Piancatelli Rearrangement

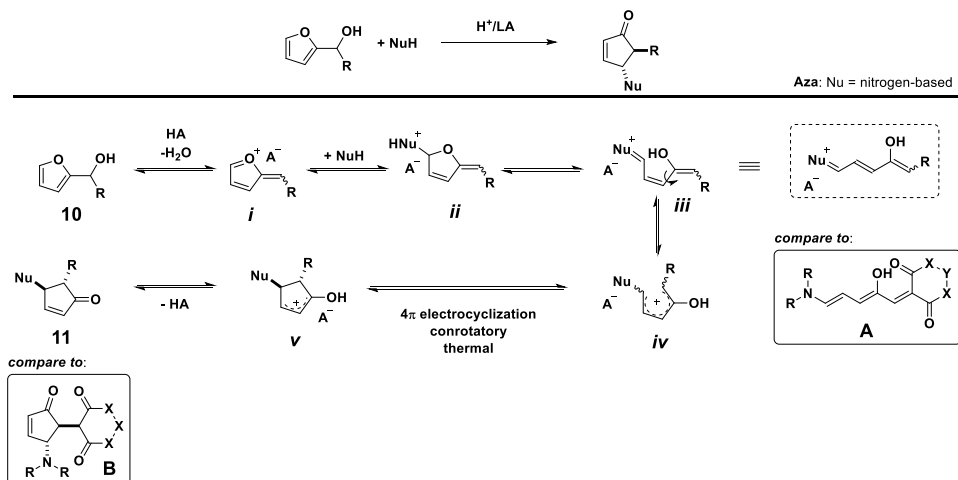


Figure 1.3 | Proposed mechanism for the (aza-)Piancatelli rearrangement.^{16,17}

So far, two generations of DASAs have been reported (Figure 1.1): first-generation compounds represented by compound **1** employ a dialkylamine donor,^{12,13} whereas second-generation DASAs represented by compound **2** employ *N*-alkyl anilines.^{14,15} Amines with strongly electron-withdrawing groups are not nucleophilic enough for ring-opening, even not at elevated temperatures. For anilines, the reaction proceeds, but slowly, so longer reaction times, additional base, excess of the amine or higher temperatures are necessary. Excess of the amine can be detrimental, as when the reaction mixture is concentrated after completion of the reaction, nucleophilic addition to the polyene chain can cause degradation and side-product formation.^{14,15} Thus, synthetic procedures of second-generation DASAs usually include a precipitation or trituration step to remove the anilines from the product.^{14,15} DASA compounds show rather limited stability on acidic silica gel upon flash column chromatography. The scope of possible nucleophiles is illustrative (*vide infra*, chemical sensing) and the reactivity of amines for ring-opening of **6** are (from slowest to fastest):¹⁹ ammonia \ll butylamine \sim cadaverine $<$ spermidine \ll diethylamine \sim dimethylamine $<$ piperidine. Other nucleophiles such as alcohols, thiols or phosphines were not able to promote ring-opening. Read de Alaniz and co-workers have reported that the stability of DASAs based on primary amines is reduced, whereas secondary amines show good stability of the elongated compound.¹³ The limitations of the current synthetic approach – despite its convenience – call for development of novel synthetic routes that do not make use of the ring-opening reaction of activated furans.

1.3 Photoswitching

The isomerization mechanism of a given class of photoswitches sets the basis for the understanding of how it responds to its environment and different experimental conditions.

Only recently, initial studies on the photoswitching mechanism have been reported.^{20–22} However, the discussion will be restricted to mechanistic aspects vital for effective and proficient handling of DASAs for applications. Starting with a static picture of DASAs, their spectral shape and their solid-state structure, the photoswitching process will then be described. In the subsequent section, applications of DASAs are illustrated and design principles are highlighted.

1.3.1 The absorption spectrum

The absorption spectrum of DASAs has two components (Figure 1.4): the absorption of the acceptor component (Meldrum's acid or 1,3-dimethyl barbituric acid; **red**, highlighted for **1B**) and the absorption of the triene push-pull chromophore (**olive**, highlighted for **1A**). The activated di-carbonyl structure in the cyclic acceptor absorbs in the UV-region of the spectrum (band around 265 nm, depending on the solvent). In toluene, where reversible photoswitching of DASAs is observed, this absorption overlaps with the solvent absorption. For second-generation DASAs, the aniline moiety also absorbs in this region.

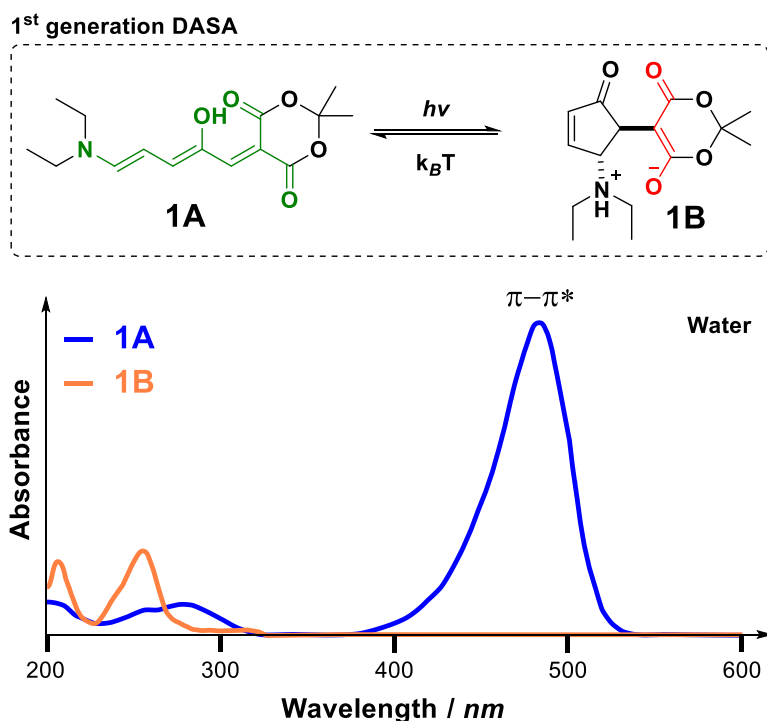


Figure 1.4 | Schematic representation of the absorption spectrum of compound **1** for both the elongated triene form (**A**) and the cyclopentenone form (**B**) in water. The push-pull system (**olive** in **1A**) and the 1,3-dicarbonyl system (**red** in **1B**), are highlighted. Adapted with permission from ref. 20. Copyright© 2016, American Chemical Society.

The triene push-pull chromophore, reminiscent of merocyanine dyes, has a strong absorption band in the visible corresponding to the π - π^* transition. For DASAs, this band lies around 450 – 700 nm. In polar protic solvents, a broadening of the band with concomitant blue-shift of the absorption maximum is observed. Importantly, DASAs exhibit almost no absorption (low ϵ and ϕ) between the UV-absorption (below 300 nm) and the visible light absorption (above 450 nm) regions, thus offering a photochemical window for operation of other processes; a fact that can be used for wavelength selective photoswitching (*vide infra*).^{23,24}

Photoswitching breaks the conjugation of the push-pull chromophore that was responsible for the visible light absorption and leads to the cyclopentenone structure **B**. This results in the loss of the strong red-shifted π - π^* band and thus only the UV-absorption of the aniline/cyclic acceptor remains. Overall, this behavior renders Stenhouse photoswitches negative photochromes,^{2,11} preventing bi-directional photoswitching so far. Switching back with light would require a cyclopentenone that shows a LUMO with density at the bond to break (C₁-C₅, marked orange in Figure 1.1). Furthermore, using UV-light for addressing the cyclized form can lead to photodegradation.

The spectrum of DASAs can be tuned in a rational way as outlined below.

Acceptor: the acceptor plays an important role for the position of the absorption maximum (Figure 1.5). Barbituric-acid-derived DASAs (*e.g.* compound **12**) exhibit bathochromically shifted spectra by about 20-25 nm as compared to the Meldrum's acid derived DASAs (*e.g.* compound **1**, Figure 1.5).^{13,14} Importantly, compound **13** was found to have an absorption maximum shifted up to 600 nm due to extended conjugation on the acceptor side, but does not photoswitch, for reasons that remain unclear.¹³ Synthetic modifications at the nitrogen atoms of barbituric acid are well known and used. However, other acceptors – not making use of either the Meldrum's acid or barbituric acid motif – have not been successfully employed for photoswitching.

Donor: second-generation DASAs in general have a bathochromically shifted absorption band as compared to first-generation DASAs, because of the extended conjugation into the aniline moiety.^{14,21} For first-generation DASAs, changes in the alkyl chains of the amine donor have little influence on the absorption maximum (few nm). In general, electron-donating groups lead to a red-shift, whereas electron-withdrawing groups lead to a blue-shift of the DASA main absorption band.^{14,15} The electron-density of anilines as donors can be conveniently controlled with substituents in the *ortho*- and *para*-position. Herein, strongly donating groups such as methoxy- or *N,N*-dialkylamine- lead to a large bathochromic shift (Table 1.1).

DASAs with *N*-methylaniline donors undergo a much reduced spectral shift upon introduction of electron donating or withdrawing groups as compared to cyclic donors (Table 1.2).^{14,15} Read de Alaniz and co-workers have related this finding to the aniline group twisting out of plane of conjugation.¹⁴ They computed that DASAs

that employ *N*-methylaniline donors exhibit larger dihedral angles Φ_{D-A} (up to 40°), whereas DASAs with cyclic donors were found to be almost planar (see Figure 1.6). This effect also translates to calculated HOMO electron densities that show reduced overlap between donor and acceptor groups, in effect reducing the shifting effect of electron-density modulation.

Polyene linker: in analogy to cyanine dyes, one expects a spectral shift of around 100 nm per added CH group in the polyene chain.²⁵ While an extension of the polyene chain might be feasible, shortening the chain will prevent electrocyclicization to form the five-membered ring.

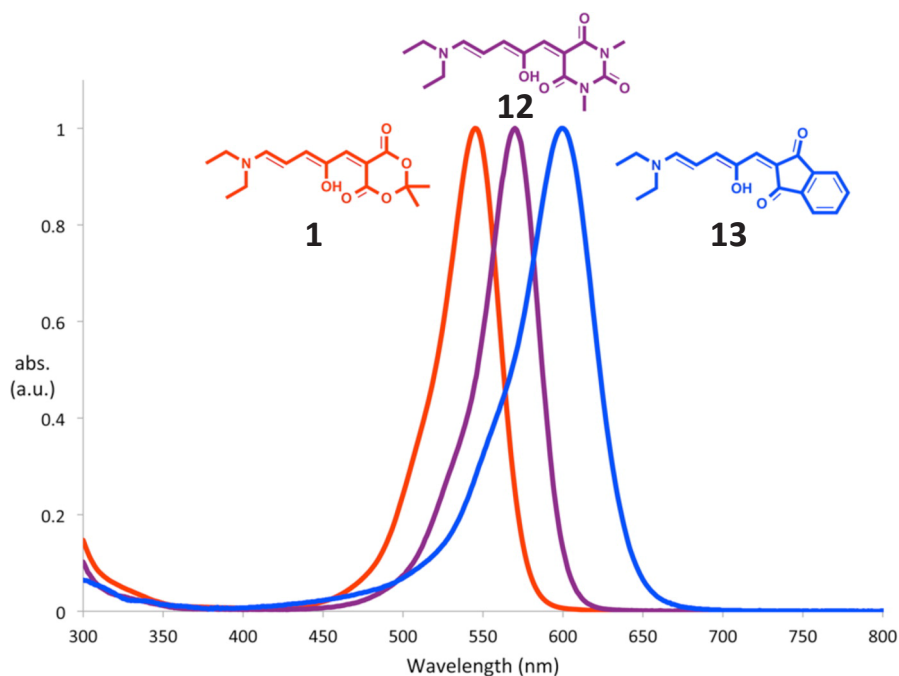


Figure 1.5 | Absorption spectra of compound **1**, **12** and **13**.¹³ Reproduced with permission from ref. 13. Copyright© 2014, American Chemical Society.

Table 1.1 | Comparison of absorption maxima of selected DASA compounds with different donor moieties in dichloromethane (in nm).¹⁴ Data taken from ref. 14.

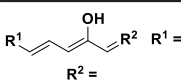
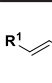
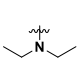
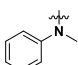
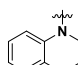
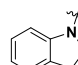
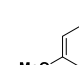
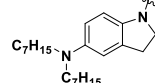
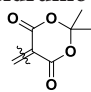
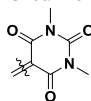
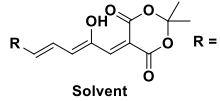
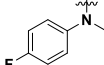
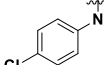
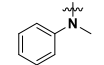
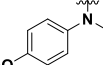
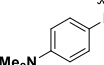
 $R^1 =$  $R^2 =$						
Meldrum's acid						
	539 ²⁰	558	575	590	603	648
barbituric acid						
	---	582	599	615	629	669

Table 1.2 | Comparison of absorption maxima of selected DASA compounds with *N*-methylaniline donors in either chloroform or dichloromethane (in nm).^{14,15} Data taken from ref. 14 and 15.

 $R =$ Solvent					
dichloromethane ¹⁴	---	558	558	561	---
CDCl₃ ¹⁵	557	---	561	563	574

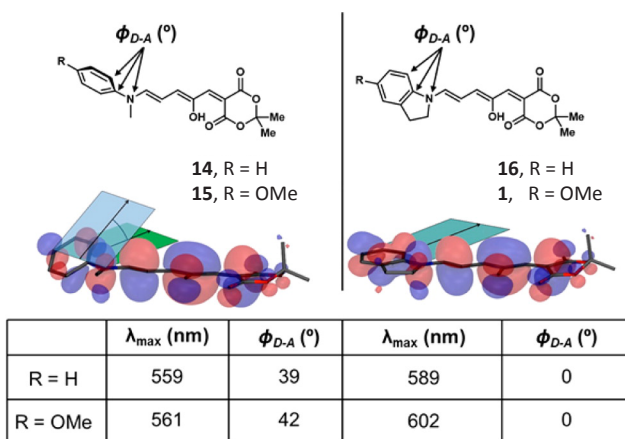


Figure 1.6 | Change of dihedral angle of the donor moiety of *N*-methyl- vs. cyclic secondary anilines affects the HOMO orbital overlap and the λ_{\max} . Reproduced and adapted with permission from ref. 14. Copyright © 2016, American Chemical Society.

1.3.2 Solid-state structures

Bond-lengths of DASAs are important for understanding the bonding character within the triene structure and thereby how difficult it is to rotate around these bonds. Bond-length alternations (BLA) give insights into the nature of the push-pull system. Generally, this structural information is accessible through crystal structures and calculations. Figure 1.7a depicts two resonance structures essential for DASAs. In crystal structures, the zwitterionic resonance structure is dominant with strong bond length alternations (BLA, Figure 1.7b).¹⁵ Computational studies support this bonding pattern.²⁶ Second-generation DASAs generally show reduced BLA.

At reduced temperature, solution ¹H-NMR spectra show that in the case of asymmetric donors ($R \neq R'$), two isomers can be observed.^{15,27} At elevated temperatures, these configurational isomers are interchangeable, in some cases leading to line-broadening.

The crystal structures of cyclized first-generation DASAs show a zwitterionic form with a clear *trans*-relationship between the donor and acceptor moiety. For second-generation DASAs, a neutral form is observed, in accordance with the $pK_{a(H)}$ values (Figure 1.8). Only for a derivative with a *p*-methoxy methylaniline donor moiety (**15**, cyclized form), the zwitterionic form is preferred, which is in contrast to the solution state.¹⁵ Beves and co-workers propose favorable H-bonding through the crystal lattice to be the cause for this change. Because of the reduced pK_{AH} value of the aniline as compared to the dialkyl amine, a zwitterionic structure is disfavored. Such changes are influential on photoswitching, as the protonation state and polarity determine the energy of the intermediate in different solvents, and thus influence equilibrium constants and photostationary states reached.

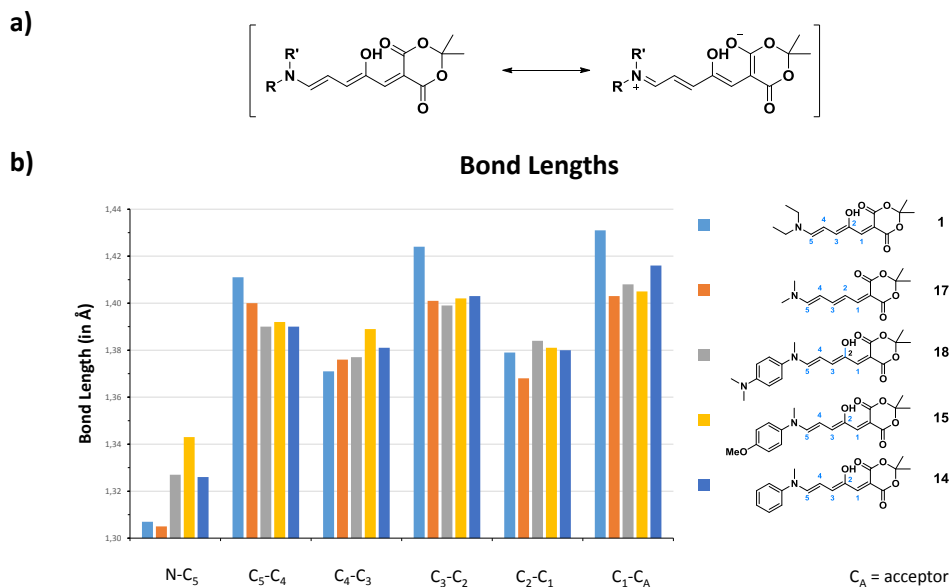


Figure 1.7 | Solid state structures of DASAs: a) possible resonance structures; b) bond-length analysis, data taken from ref. 13, 15 and 28. Adapted with permission from ref. 15, Copyright© 2016, The Royal Society of Chemistry.

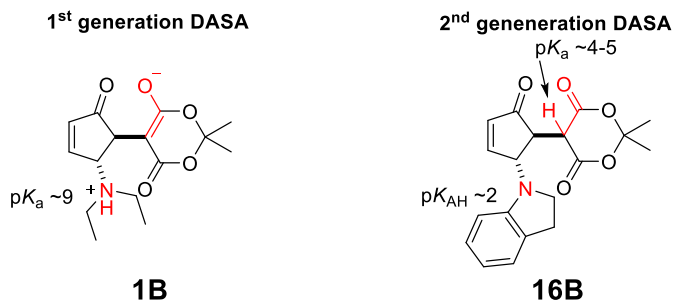


Figure 1.8 | $pK_{a(H)}$ values associated with structural elements of DASAs are responsible for differences of the protonation states in the cyclized form.

1.3.3 Photoswitching

The following represents a brief summary of mechanistic aspects of DASA photoswitching needed to understand applications described subsequently. As the main body of this thesis constitutes this mechanistic work, the reader is kindly referred to Chapter 3–5.

With an understanding of the structure and the absorption spectrum of both the elongated triene form (**A**) and the cyclopentenone form (**B**), the effect of irradiation will be discussed next. Stimulating the $\pi-\pi^*$ transition with visible light triggers a photoisomerization of one of the “double” bonds. DFT calculations provide access to bond lengths both in the ground and excited state (Figure 1.9) of both compound **1** and an analogue lacking the C_2 -hydroxy group (compound **19**).²² Notably, the presence of the hydroxy group seems to “(pre)select” the bond adjacent to it (C_2-C_3) for isomerization. Upon removal of the hydroxy group, no cyclization is observed and photoisomerization is not restricted to a single bond anymore, but is observed for C_2-C_3 and C_3-C_4 . Ultrafast pump-probe spectroscopy, NMR studies and TD-DFT calculations suggest that the hydroxy group stabilizes the ground state conformation (**A**, Figure 1.10) through a strong hydrogen bond to one of the carbonyl groups of the acceptor and exerts an electronic effect weakly on the ground state and strongly on the excited state.²² Herein, an elongation of the bond to isomerize (C_2-C_3) mainly in the excited state is observed (Figure 1.9).

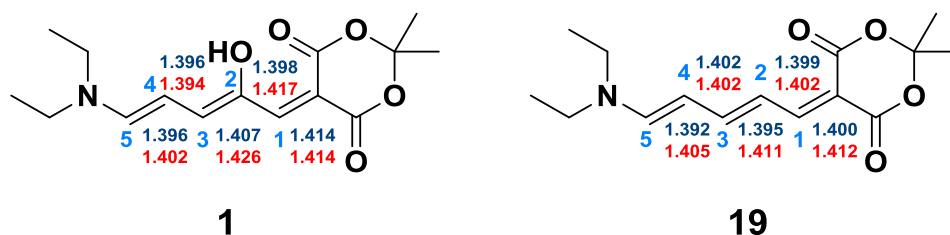


Figure 1.9 | Comparison of bond lengths (in Å) for **A** in the ground state (blue, SMD/B3LYP/6-31++G(d,p)) and excited state (red, SMD/TD-M06-2X/6-31+G(d)) in chloroform: a) for DASA **1** and b) its non-hydroxy analogue **19**. Adapted with permission from ref. ²². Copyright © 2018, American Chemical Society.

For the proposed mechanism behind the transformation of the “double”-bond-isomerized intermediate **A'** into closed cyclopentenone structure **B** (Figure 1.10), inspiration can be found in the (aza-)Piancatelli rearrangement^{16,17} and the *iso*-Nazarov cyclization.²⁹ Herein, a pentadienyl cation undergoes a thermally allowed, conrotatory 4π -electrocyclization, responsible for the formation of the five-membered-ring. Successful cyclization relies on close spatial proximity of C_1 and C_5 . After photoisomerization around C_2-C_3 (to form **A'**, Figure 1.10), spatial arrangement is not yet optimal, but a thermal rotation around C_3-C_4 does so through a twisted intermediate **A''** (Figure 1.10). Studies on the photochemical isomerization infer the presence of **A'**, which is generated on a picosecond timescale.²¹ With ultrafast time-resolved spectroscopy, **A''** and **B** are not observed, suggesting that they are not directly

involved in the actinic step (= the photochemical step). Formation of **B** relies on a proton-transfer. Experiments on the role of the hydroxy proton suggest a vital role, however the timing and nature of the proton transfer remains elusive to this point. It is not clear whether the proton highlighted as orange (Figure 1.10) is effectively staying the same, or whether protons are exchanged rapidly with the environment, as suggested by experiments in deuterated methanol.²² The cyclization step will need some more attention as mechanistic details of this step remain unknown. Notably, the presence of **A'** can be observed in time-resolved steady state UV/vis measurements, where a transient absorption band red-shifted with respect to **A** is observed.²⁰ In the case of reversible photoswitching, **B** is thermally unstable and thus can revert back to **A** through the same sequence of steps. Intermediate absorption bands are not observed for back-switching in photoaccumulation UV/vis experiments, presumably because the steady state concentration of these intermediates is too low to be observed, as the isomerization is faster than the ring-opening.²⁰ While the reversible photoisomerization itself is fast (picosecond timescale), the electrocyclization step is most likely the rate-limiting step in photoswitching experiments. Because the back-reaction (from **B** to **A'** to **A**, Figure 1.10) is thermally controlled, reducing the temperature leads to accumulation of either **A'** or **B**, depending on the experimental setup and temperature. Photoaccumulated **A'** could be selectively probed with pump-probe spectroscopy showing that irradiation at the **A'** absorption band results in back-isomerization to **A**.²¹ Photoaccumulated **B** can be used in applications (*vide infra*): Hooper and co-workers for instance used cross-linked polyurethane elastomers doped with first-generation DASAs to measure temperature jumps by making use of the re-colouring back-reaction from **B** to **A**.³⁰

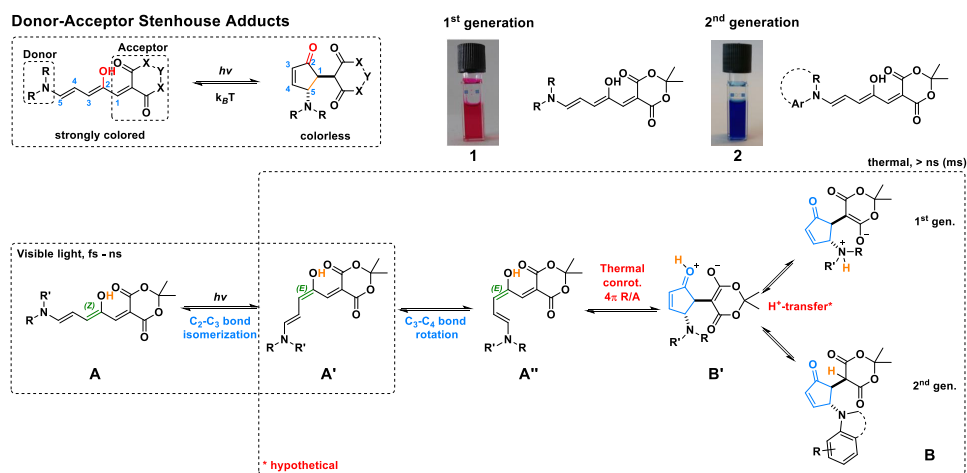


Figure 1.10 | Proposed photoswitching mechanism of donor-acceptor Stenhouse adducts. Adapted with permission from ref. 21, Copyright © 2017, American Chemical Society.

In summary, the current mechanistic hypothesis (Figure 1.10) divides photoswitching into a light-driven part (actinic step), followed by a series of thermal steps including a thermally allowed, conrotatory 4π -electrocyclization (Figure 1.10). Upon irradiation, a “double”-bond isomerization occurs on the bond adjacent to the hydroxy group (C_2 - C_3 , green) to yield **A**. Through the presence of the hydroxy group, the triene chain gets polarized in such a way that isomerization around the C_2 - C_3 bond is favored as compared with other possible bond isomerizations. This mechanistic proposal is based on investigations by NMR, UV/vis steady state spectroscopy, ultrafast time-resolved UV/vis and mid-IR spectroscopy and variable temperature experiments. The proposed photoswitching mechanism sets the basis for further discussion: the energy levels of each of the intermediates involved is dependent on the solvent and possibly the environment (*e.g.* surface or packing). These intermediates differ quite drastically in charge, polarity, dipole moment and geometry and their energy levels can differ remarkably, thus changing the overall switching properties from solvent to solvent (see section 1.3.6).

1.3.4 Cyclization under exclusion of light

Light as a stimulus is not needed in all cases: especially in polar protic solvents (*e.g.* water and methanol), a background reaction from **A** to **B** (Figure 1.10) in the dark is observed, where the compound undergoes cyclization independently of light. On a mechanistic level, it is so far not understood how this cyclization is facilitated. For second-generation DASAs in all solvents studied, an equilibrium between **A** and **B** exists and these equilibria differ from solvent to solvent (Figure 1.11) and vary for different acceptors (Figure 1.12).^{14,15}

Read de Alaniz and co-workers suggest that the equilibrium of **A** and **B** roughly correlates with the pK_{AH} of the donor moiety in case of second-generation DASAs (Figure 1.11).¹⁴ With increasing basicity, the amount of elongated triene increases in for instance dichloromethane. Furthermore, these equilibria are temperature dependent.¹⁵

1.3.5 Kinetics of cyclization and ring-opening

Generally, the observed switching kinetics for both cyclization and ring-opening are strongly dependent on the solvent (see section 1.3.6). For first-generation DASAs, compounds based on dialkyl barbituric acid show a higher thermal re-isomerization rate than the corresponding Meldrum's acid-based compounds, as exemplified by the comparison of compound **1** and **12**.¹² Second-generation DASAs are recolouring more slowly than first-generation DASAs in toluene. The electronic properties are influencing the photoswitching markedly, as can be seen in Table 1.3.¹⁵

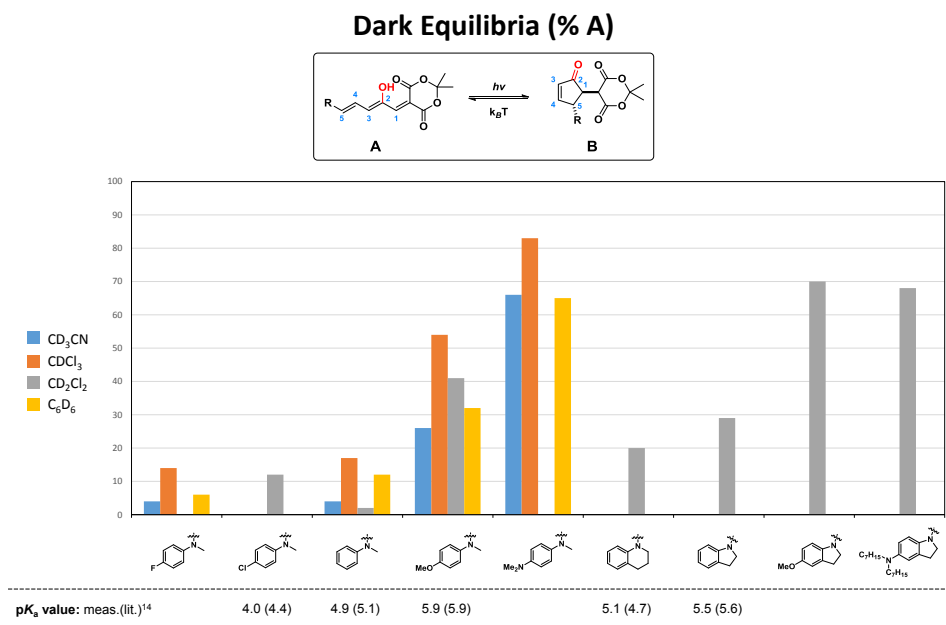


Figure 1.11 | Comparison of equilibria (in % A) of selected DASA compounds with different donor moieties as a ratio of elongated (A) to cyclized (B) determined by 1H -NMR. Data taken from ref. 14 and ref. 15.

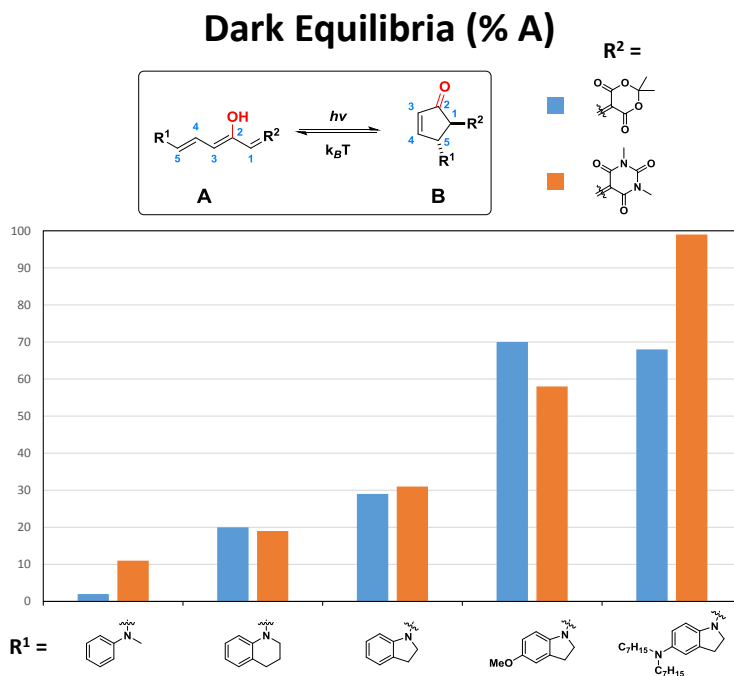
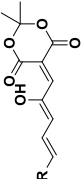
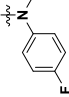
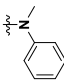
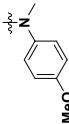
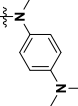


Figure 1.12 | Comparison of the influence of acceptors on equilibria (in % **A**, in CD_2Cl_2) of selected DASA compounds with different donor moieties as a ratio of elongated (**A**) to cyclized (**B**) determined by $^1\text{H-NMR}$. Data taken from ref. 14.

Table 1.3 | Comparison of absorption maxima, equilibrium constants and kinetic constants of DASA compounds with *N*-methylaniline donors in deuterated acetonitrile, chloroform and benzene. Table adapted with permission from ref. 15 Copyright© 2016, The Royal Society of Chemistry.

Solvent	CD ₃ CN	CDCl ₃	C ₆ D ₆						
 Donor, R = <div style="display: flex; justify-content: space-around; align-items: center; margin-top: 10px;"> <div style="text-align: center;">  </div> <div style="text-align: center;">  </div> <div style="text-align: center;">  </div> <div style="text-align: center;">  </div> </div>	A:B	A:B (PSS)	<i>t</i> _{1/2} [min] ^[a]	A:B	A:B (PSS)	<i>t</i> _{1/2} [min] ^[a]	A:B	A:B (PSS)	<i>t</i> _{1/2} [min] ^[a]
	4:96	0:100	5.8	14:86	0:100	57	6:94	0:100	ND ^[c]
	4:96	0:100	5.8	17:83	0:100	21	12:88	0:100	ND ^[c]
	26:74	10:90	9.9	54:46	0:100	12	32:68	0:100	194
	66:34	65:35	ND ^[b]	83:17	80:20	4.7	65:35	0:100	17

ND = Not determined. [a] Apparent half-life times: time form PSS to halfway to dark equilibrium; [b] change in equilibrium too small; [c] thermally stable, kinetics too slow for rate determination (298 K, observed for 100 to 180 min).

1.3.6 Solvent effects

With a more thorough understanding of the proposed photoswitching mechanism in hand, solvent effects on first and second-generation DASA photoswitching can be discussed. Photoswitching of first-generation DASAs (e.g. compound **1**) is highly solvent dependent (Figure 1.13).^{12,13} in polar protic solvents, photoswitching from **A** to **B** is irreversible (Figure 1.13a) and a background reaction under exclusion of light is observed (*vide supra*), since energetically the zwitterionic form **B** is favored in polar solvents. This behavior was originally used to isolate and study the cyclic **B** form.^{12,13} In chlorinated solvents such as chloroform or dichloromethane, no or very little photobleaching, rather reversible photoisomerization is observed.^{20,21} The observed photoswitching resembles that of the non-hydroxy analogue **19** (*vide supra*).²² For compound **1**, reversible photoswitching is observed only in aromatic solvents such as toluene or benzene. Notably, the rate of photoswitching across solvents differs. While in toluene photobleaching occurs rapidly, polar protic solvents decelerate this process dramatically.²⁰ The observed bathochromically (with respect to the main absorption band, **A**) shifted transient absorption band, indicative for **A'**, is not apparent in photo-accumulation experiments in polar protic solvents.

Considerations of solvent effects on photoswitching are essential for devising successful applications. The system that needs to be controlled by light determines the environment the photoswitch will be embedded in and will determine its photoswitching behavior. Thus, understanding solvent effects and being able to make use of them according to one's needs influences the success of the applications. A premier example on how knowledge of the behavior of first-generation DASAs has been used productively are phase-transfer experiments:^{13,31} the solvent dependent behavior of first-generation DASAs is largely a result of the zwitterionic **B** form.^{13,23} The elongated triene form **A** is neutral; upon photoswitching it forms the zwitterionic form **B** that is thermally unstable and prefers a more polar environment. Photoswitching thus results in dynamic phase transfer from the organic phase into an aqueous phase, if present nearby. This dynamic phase-transfer can be used for extraction experiments, where the toluene phase discolors upon photoswitching and the aqueous phase turns yellowish because of the presence of **B**.^{13,23} **B** is stable in aqueous environments and thus does not spontaneously open up to **A**. The **A** form can be recovered by back-extraction with dichloromethane. In this environment, **A** is favored and the compound will ring-open again.

Interestingly, it is the hydrophobicity/hydrophilicity of the amine donor that dictates the efficacy of the phase transfer (Figure 1.13b).¹³ DASAs bearing a short alkyl chain amine donor (e.g. diethyl- or di-*n*-butylamine) quantitatively transfer to the aqueous phase upon irradiation. Conversely, a long alkyl chain donor-derived DASA (e.g. di-*n*-octylamine), undergoes photocyclization but fails to transfer to the aqueous phase. This phenomenon is reversed during the recovery with halogenated solvents, where the cyclized form may be removed from the aqueous phase after photoinduced transport. Here, the shortest alkyl chain donor DASA (diethylamine) is only recovered in 10%, while the moderate length donor DASA (di-*n*-butylamine) is recovered near quantitatively. The donor and acceptor moiety (especially for 1,3-dialkyl barbituric acid) allow convenient modification and thus tuning of

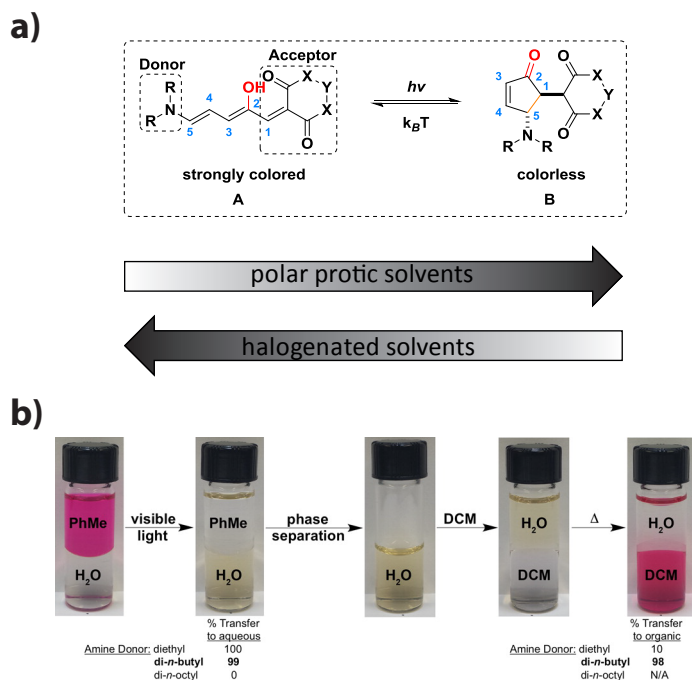


Figure 1.13 | Solvent effects on first-generation DASA photoswitching: a) polar protic solvents stabilize **B**, whereas halogenated solvents stabilize **A**; b) the strong difference in polarity upon photoswitching enables phase transfer of the compound. N/A = not available. Adapted with permission from ref. 13. Copyright © 2014, American Chemical Society.

polarity of the compound. Even amphiphiles have been obtained and used for phototriggered disassembly of micelles (*vide infra*).^{12,32} Because of their different pK_a values, second-generation DASAs (*e.g.* compound **2**) form a neutral **B** form, thus avoiding such pronounced solvent effects.^{14,15} The presence of the aromatic donor, however, generally reduces solubility in polar protic solvents.

In summary, taking into account solvent effects on DASA photoswitching is an essential prerequisite for successful applications. The overall behavior of the compound in question is determined by the individual energies of the intermediates involved in the photoswitching mechanism and the energetic barriers between them. More work has to be done to disentangle different effects governing these behaviors.

1.4 Illustrative Applications

With a better understanding of DASA photoswitching and properties in hand, the following section will discuss applications of DASAs and how these properties have been employed.

1.4.1 Drug delivery

First-generation DASAs show a large change in structure and polarity upon photoswitching. Such a molecular contraction can be used to disrupt aggregates: with a hydrophilic tail at the donor end, and long alkyl chains on the 1,3-dialkyl barbituric acid acceptor, an amphiphile was created that can assemble into micelles (Figure 1.14a). Irradiation leads to photo-disassembly of such micelles as show-cased by Read de Alaniz, Hawker and Soh and co-workers (Figure 1.14b).^{12,32} In this case, 1,3-dialkyl barbituric acid (**20**: octyl-; **21**: dodecyl-) served as an acceptor for the non-polar side and a clickable PEG-chain ($M_w = 3000$ g/mol, PDI = 1.1)¹² was used for the polar end. Nile red can be used to study micelle behavior. Upon incorporation into lipid membranes Nile red undergoes a large blue-shift and fluorescence enhancement as compared to polar solvents. Disassembly releases the dye, which leads to a drop of fluorescence and red-shift. Dynamic light scattering and incorporation of Nile Red in the micelles confirmed both the formation of micelles (critical micellar concentration $CMC(\mathbf{20}) = 49 \mu\text{M}$) in aqueous environments and cargo-release upon photocyclization. In polar solvents, such as aqueous solutions used in this study, first-generation DASAs cyclize irreversibly.¹³ This irreversible cyclization is also observed in the micellar system, where irradiation led to complete disappearance of the visible light absorption band around 550 nm and was not recovered in time.

Increasing the hydrophobic acceptor part (compound **21**, Figure 1.14a) lowers the CMC to $8.5 \mu\text{M}$ and increases the stability of the micelle (average size ~ 22 nm in diameter).³² The DASA-based micelles were used to deliver cargo to cells (Figure 1.14c). Importantly, the cyclized amphiphile does not hinder cargo distribution and the amphiphile does not reduce cell viability.³² The chemotherapeutic agent paclitaxel was successfully delivered to MCF-7 human breast cancer cells (Figure 1.14d) and cell viability assays show the effect of paclitaxel release (0.17 wt% drug loading) upon irradiation. Interestingly, the assembled micelles seem unaffected by ambient light for shorter time-periods (<3 h). Photoswitching of the DASA moieties in micelles under irradiation (see Figure S3 of ref 32; $\lambda_{\text{max}} = 553$ nm in water, 0.5 mg/mL, white light: $\lambda = 350\text{--}800$ nm, maximum 0.9 mW cm^{-2}) is relatively slow in bulk (~ 1 h). Overall, the described approach offers advantage over some existing micellar systems making use of irreversible uncaging^{3,4} by allowing visible light control.

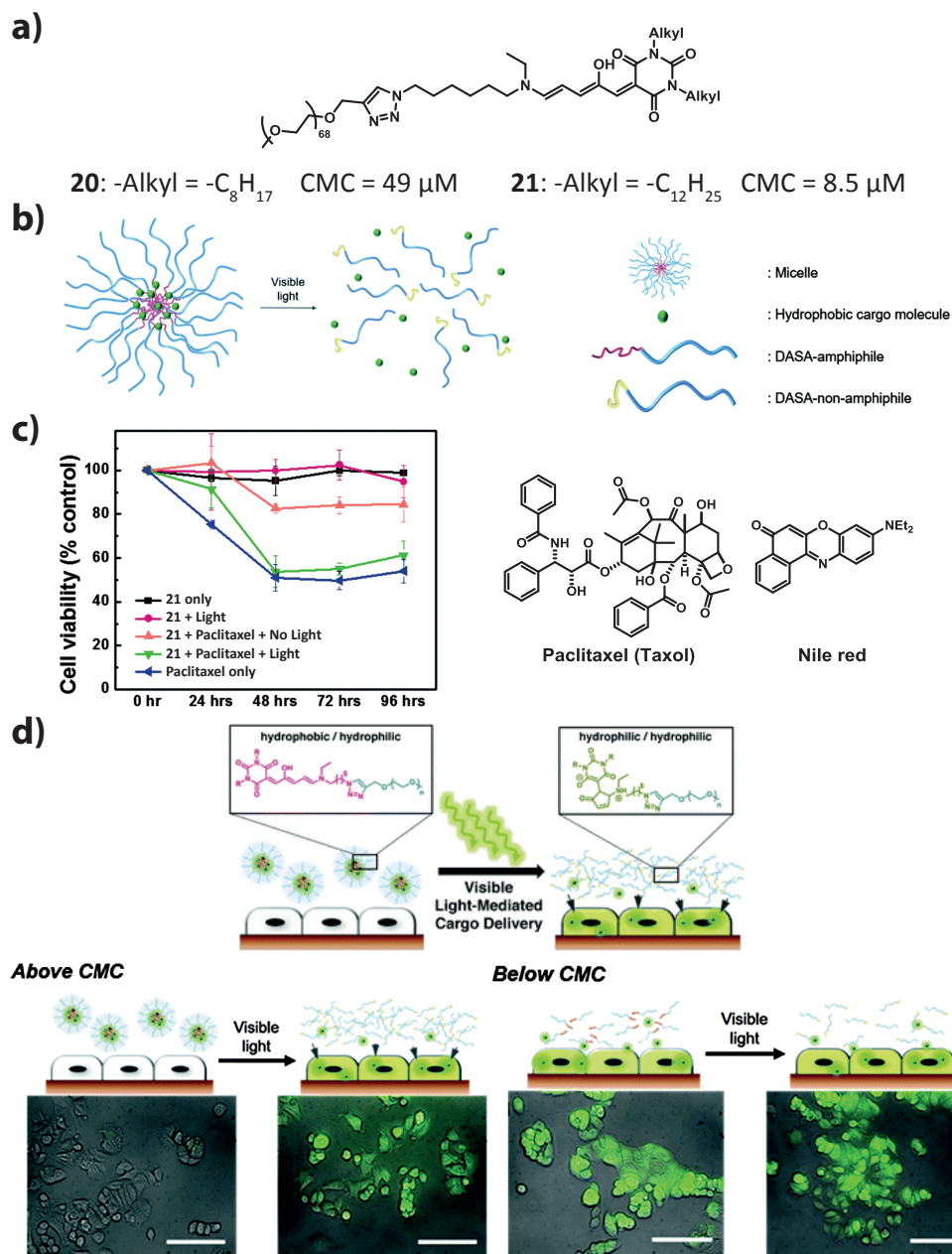


Figure 1.14 | DASAs for visible-light mediated release of cargo from micelles: a) DASA-based amphiphiles and their associated CMC; b) concept of light-switchable cargo-release; c) *in vivo* assays using MCF-7 cells and Nile-red; d) cell-viability assay with paclitaxel. Adapted with permission from ref. 32. Copyright[©], 2016, Royal Society of Chemistry.

1.4.2 Dynamic phase-transfer for catalyst recycling

Read de Alaniz and co-workers devised a recyclable organo-catalyst for a thiourea-catalyzed lactide polymerization based on first-generation DASAs (Figure 1.15), making use of the large change of polarity upon photoswitching.³¹ Herein, a DASA tag was attached to a thiourea-based organocatalyst, using a click-reaction to form **22**. Under light-irradiation, the catalyst could be separated from the reaction mixture and then reused. Catalyst **22** was found to promote polymerization and lead to polymer conversions of 60-70% within 48 h, PDIs of

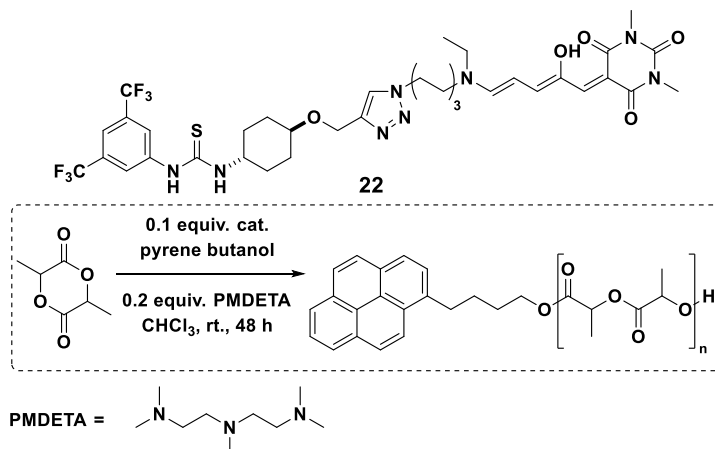


Figure 1.15 | DASA-based recyclable thiourea catalyst for lactide polymerization. Adapted with permission from ref. 31. Copyright[©], 2015, ScienceDirect, Elsevier.

1.12–1.31 and molecular weights of 8.1–11.2 kg/mol in three subsequent cycles of catalysis and catalyst recovery. The authors note that catalyst separation could be useful to reduce transesterification reactions and potential polymer degradation.

1.4.3 Applications in polymers and on surfaces

DASAs undergo photobleaching upon irradiation that can be used to create patterns on surfaces with high spatial precision. In 2015, Singh *et al.* reported the functionalization of a polycarbonate surface with DASA molecules, where lithographic masks were used for photopatterning (Figure 1.16).³³ Polycarbonate foils were functionalized with branched polyethyleneimine (Figure 1.16a). The free primary and secondary amines were then used to open up the furfurylidene group (**6**) to generate DASA groups **23** at the surface. The DASA-containing surface was rendered photoresponsive (Figure 1.16b), but the photoswitching was irreversible, which might stem from the polar environment of the surface due to the layer of polyamines. The surface modification and formation of the cyclized form **23B** upon irradiation was studied thoroughly by ¹H-NMR, ATR-IR, ToF-SIMS and XPS techniques. With the large change of polarity, a change of surface wettability (as analyzed by contact angle measurements: before irradiation = 74.2°; after irradiation = 56.3°) was achieved.

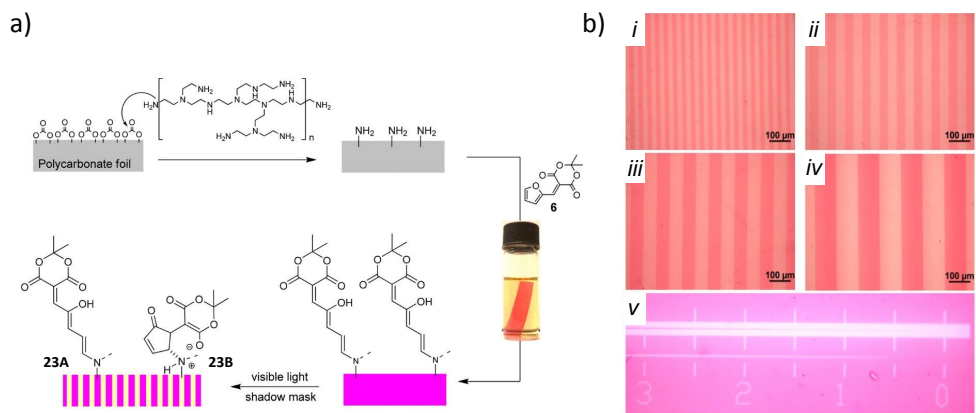


Figure 1.16 | Covalently attached first-generation DASA **23** on a polycarbonate surface: a) synthesis and b) surface patterning. Patterns obtained after 18 h of irradiation with linewidths of 20 μm (*i*), 40 μm (*ii*), 60 μm (*iii*), 100 μm (*iv*) and using a photolithographic test mask (*v*, 3 μm – submicron scale). Adapted with permission from ref. 33. Copyright[©], 2015, American Chemical Society.

A similar approach was taken by He and co-workers (Figure 1.17)³⁴ who studied a polystyrene-based polymer with attached DASA groups in solution and spin-coated on surfaces. Upon irradiation, a change in surface wettability and color pattern is observed. A poly(styrene-*co*-4-vinylbenzyl chloride) polymer was synthesized by radical polymerization of **24** and **25**. Subsequent functionalization of the vinylbenzyl chloride moieties (1:5 ratio with respect to styrene) with *n*-butylamine rendered the polymer suitable for DASA synthesis using the activated furan **6** to form DASA **26** attached to the polymer. Upon irradiation of the spin-coated polymer on quartz slides, a change of the water contact angle from 93.4° to 72.6° was observed. As before, the photoswitching is irreversible in the polymer, which is surprising giving the apolar environment.

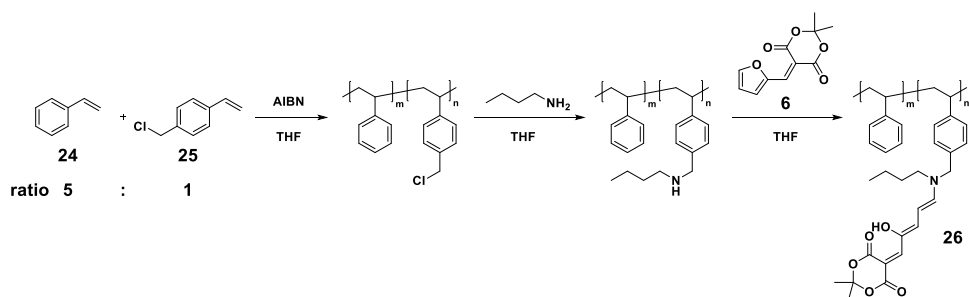
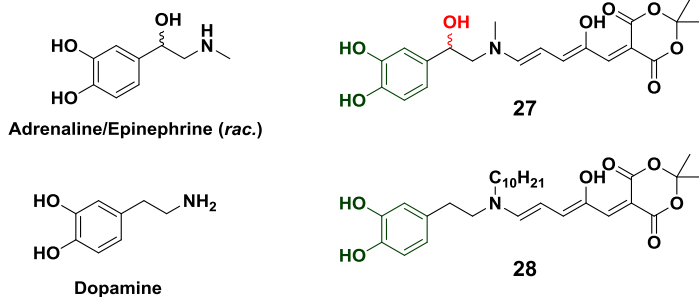


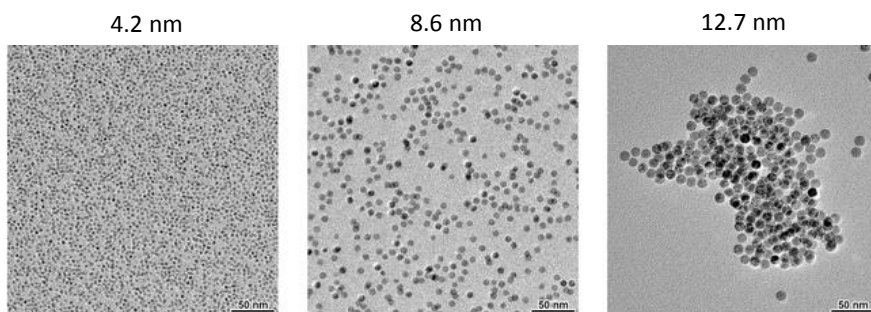
Figure 1.17 | Functionalization of a poly(styrene-*co*-4-vinylbenzyl chloride) polymer with first-generation DASAs. Adapted with permission from ref. 34. Copyright[©], 2016, Wiley-VCH Verlag GmbH & Co. KGaA.

a)



b)

Fe_3O_4 nanoparticles functionalized with **28**



c)

spontaneous photobleaching

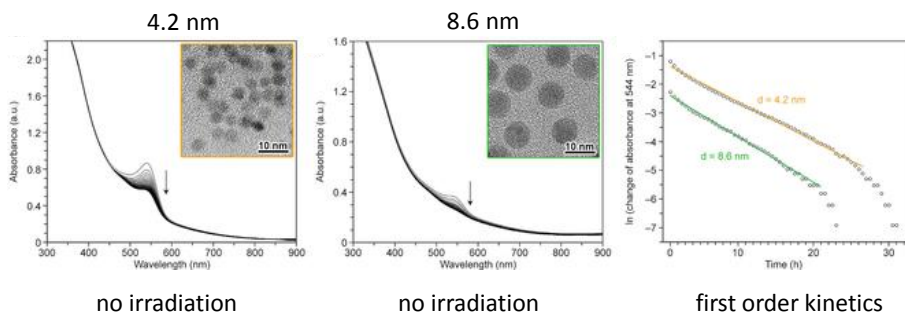


Figure 1.18 | Catechol containing DASAs **27** and **28** for surface functionalization of magnetite nanoparticles: a) molecular structure of DASAs **27** and **28**; b) TEM images of magnetite nanoparticles of different size functionalized with DASA **28** in toluene; c) bleaching of the DASA absorption band without irradiation on the surface of magnetite nanoparticles of 4.2 nm and 8.6 nm diameter over the period of several hours [nanoparticles] = 0.25 mg mL⁻¹. The time-evolution of absorbance follows first order kinetics. Adapted with permission from ref. 27. Copyright©, 2017, Wiley-VCH Verlag GmbH & Co. KGaA.

The problem of irreversible photoswitching in polar environment has also been encountered by Klajn and co-workers (Figure 1.18).²⁷ Based on previous extensive work on inorganic nanoparticles modified with responsive elements to create out-of-equilibrium systems, they set out to attach DASA-photoswitches to magnetite (Fe_3O_4) nanoparticles by extending the amine donor with a 1,2-dihydroxybenzene unit to yield compounds **27** and **28**. Nanoparticles were modified with either compound **27** or **28** (Figure 1.18a and b), and their behaviour was found to differ dramatically: the small methyl group in **27** facilitates ring-closure and upon addition of **27** to oleate-protected magnetite nanoparticles and purification, the resulting solids were insoluble.²⁷ Photoswitch **28**, on the contrary, contains an alkyl chain for solubilisation and lacks a hydroxy group in the donor part, solving some of the problems encountered before, but resulting in reduced switching capabilities in solution inferred by slow switching under irradiation and low photostationary states reached. Even in non-polar solvents, this first-generation DASA photoswitch existed in an equilibrium (open-closed), which is unusual.^{12–15,20} Notably, a small absorption band at 620 nm (Figure 1.19) is observed in solution in toluene and dichloromethane, possibly representing an intermediate in the photoswitching mechanism stabilized by an interaction between the catechol moiety and the Meldrum's acid part. This is not the case in methanol. Upon surface immobilization, the catechol group would be involved in the surface binding, removing such caveats. However, once functionalized, these magnetite particles showed irreversible, spontaneous photobleaching (Figure 1.18c). Interestingly, Klajn and co-workers find that a possible (anti-parallel) intercalation of DASA moieties seems to slow down their cyclization on the surface by stabilizing the elongated triene form. They further noted a slow bleaching reaction of DASAs in glass vials initiating at the glass surface (see SI Figure S6 of ref. 27). The authors conclude that cyclization is promoted by both polar surfaces such as glass and neighbouring cyclized zwitterionic DASAs.

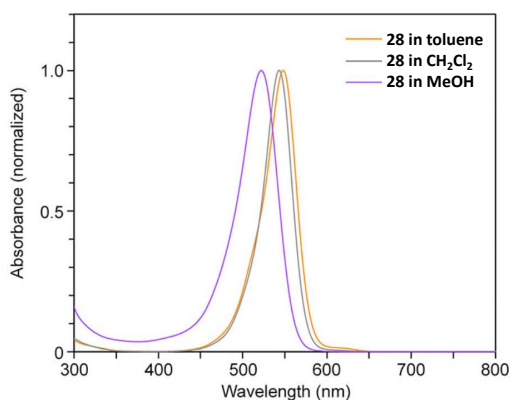


Figure 1.19 | Absorption spectra of compound **28** in different solvents: the small absorption band around 620 nm highlighted by the authors is observable in non-polar solvents and chlorinated solvents, but not polar protic solvents. In toluene, irradiation does not change the position or the amount of the small absorption band. Adapted with permission from ref. 27. Copyright ©, 2017, Wiley-VCH Verlag GmbH & Co. KGaA.

Importantly, there have been examples that allow for reversible DASA photoswitching in polymers: in 2016, Hooper and co-workers doped a polyurethane-based elastomer with di-*n*-octylamine based DASA **29** (Figure 1.20),³⁰ using the long alkyl chains to increase solubility. The so-obtained gel remained colorless upon storage in cooled environment, but showed temperature-dependent re-coloration upon heating. This temperature dependent-recoloration enabled heat-mapping of peak temperature of ballistic entries into the polymer. The DASA photoswitch was uniformly distributed in the gel and showed no agglomerates, enabling a high spatial resolution of the temperature history of the elastomer. Prolonged irradiation of a heated sample results in re-cyclization of DASA and partial decomposition of the photoswitch. It is remarkable that the relatively non-polar hydroxyl-terminated polybutadiene (HTPB)-based crosslinked polyurethane polymer allows thermal cycloreversion and thus re-coloration.

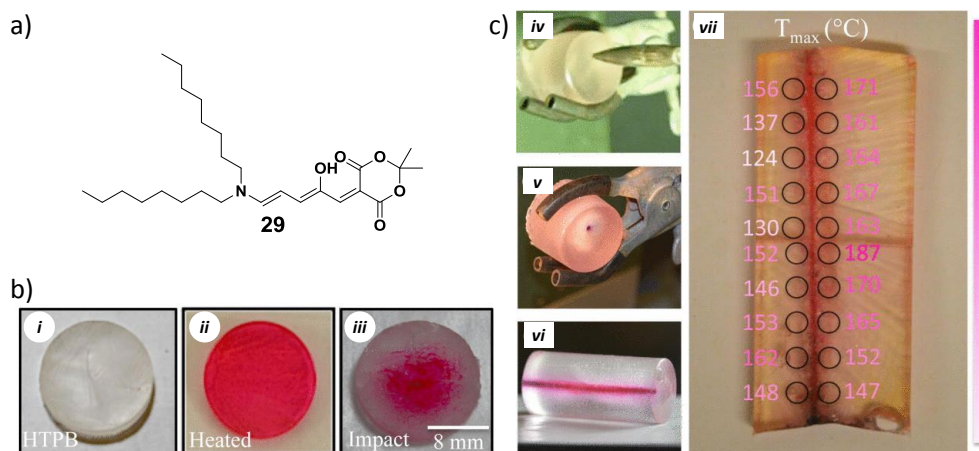


Figure 1.20 | Temperature mapping using DASA **29** (a) in a hydroxyl-terminated polybutadiene (HTPB) polymer crosslinked with hexamethylene diisocyanate (b): (i) irradiated, (ii) heated and (iii) impacted (Hopkinson bar compression). c) temperature mapping after projectile impact on the elastomer: (iv) before, (v and vi) after bullet perforation, (vii) calculated peak temperatures in cut open polymer. Adapted with permission from ref. 30. Copyright©, 2016, AIP Publishing LLC.

As the cyclopentenone form **B** of second-generation DASAs is neutral and not zwitterionic (Figures 1.8 and 1.10), irreversible photoswitching in polar media due to polarity can be avoided. To that end, the groups of Boesel and Read de Alaniz synthesized a range of acrylate and methacrylate polymers bearing 3–4 mol% of a first-generation DASA **30** or different secondary DASA groups **31–34** covalently attached (Figure 1.21a).³⁵ Functionalization made use of displacement of a pentafluorophenyl ester with a primary amine (Figure 1.21b). DASAs were incorporated into poly(methyl acrylate) (PMA), poly(butyl methacrylate) (PBMA), poly(propyl methacrylate) (PPMA) and poly(ethyl methacrylate) (PEMA) polymers. Second-generation DASAs exist in an equilibrium between the open form **A** and the neutral closed form **B** strongly depending on the solvent, also in the polymer (*vide supra*, section 1.3.4).

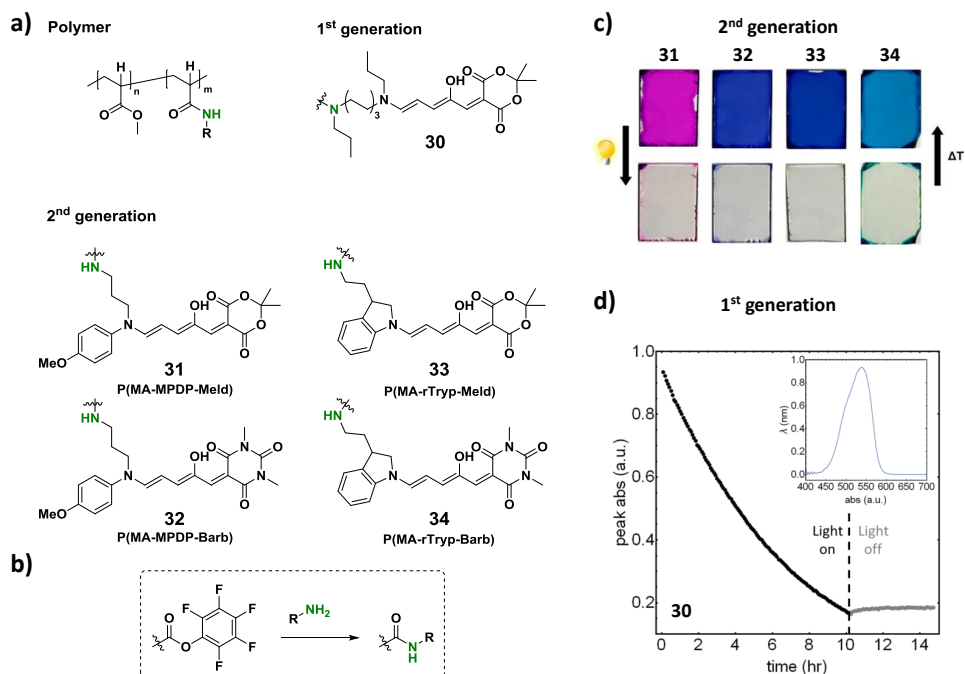


Figure 1.21 | Photoswitching of DASA-polymer conjugates: a) the PMA polymer, first-generation DASA **30** and second-generation DASAs **31–34** used; b) the functionalization method; c) reversible photoswitching of the second-generation DASA moieties covalently attached to the PMA polymer matrices in thin films (DASAs **31–34**); d) for comparison irreversible photoswitching of a first-generation DASA–PMA conjugate (**30**). Adapted with permission from ref. 35. Copyright©, 2017, American Chemical Society.

Irradiation of spin-coated polymers with white light leads to full photobleaching, which could be reversed upon heating (Figure 1.21c). The polymer matrix state (rubbery vs. glassy) influences photoswitching kinetics, as the glassy state seems to trap the cyclized form effectively preventing ring-opening to a large extent. Reversible photoswitching was not possible with first-generation DASA **30** (Figure 1.21d).

In summary, DASAs are ideally suited for responsive materials, where their strong change in color and molecular properties upon photoswitching can be harnessed. A current limitation of first-generation DASAs is the irreversible photobleaching in polymers and on surfaces. This can be overcome in apolar environments and by DASAs not being covalently attached to the surface or polymer. Second-generation DASAs do not generate a zwitterionic **B** form upon cyclization allowing for reversible photoswitching even in polymers. It has to be taken into account, however, that they exist in an equilibrium between the open form **A** and the closed form **B**.

1.4.4 Liquid crystals

DASAs have also been employed in liquid crystalline systems (Figure 1.22).³⁶ Graham, Boyd and co-workers have reported a lipid-based lyotropic liquid crystalline mesophase in water using phytantriol as the liquid crystal matrix and DASA 35 as a dopant (Figure 1.22a). The order of the liquid crystalline system also changes with temperature. The transition temperature for order-order phase changes decreases with increasing amount of the photoswitch present (above 2.5%). Upon irradiation with 532 nm light at 37 °C, an order-order phase transition was observed, which was strongly dependent on the DASA concentration, with higher concentrations leading to a larger change of lattice parameters and phase (Figure 1.22b). At $\leq 0.5\%$ DASA dopant, an incomplete, but reversible change from the bicontinuous cubic phase (V_2) to the hexagonal phase (H_2) was observed. Higher DASA concentrations would promote complete phase transitions (2.5% DASA), which turns irreversible at 5% and extends to $V_2 \rightarrow H_2 \rightarrow L_2$ (reverse micelle). Despite some reversible order-order phase transitions for

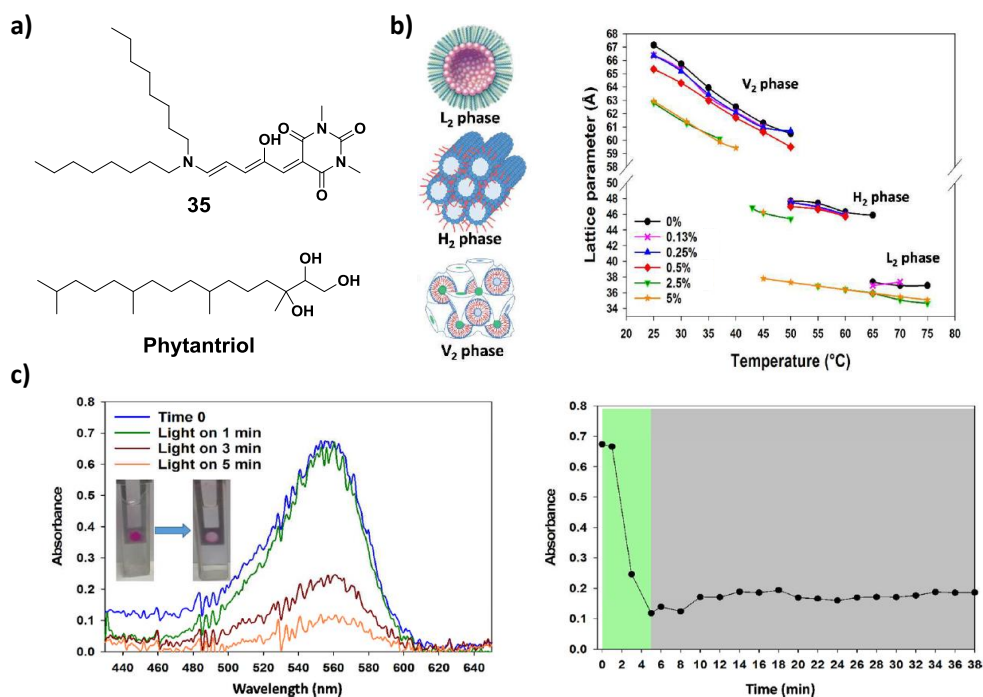


Figure 1.22 | DASA 35 in a lipid-based lyotropic liquid crystalline mesophase in water: a) structures of phytantriol and DASA 35; b) temperature dependent phase-transitions of the mesophase with illustrations of the different phases; c) absorption spectra of the liquid crystalline system doped with DASA under irradiation (532 nm) and the evolution of the UV-signal at 560 nm in time during and after cessation of irradiation. Very little recovery of absorbance is observed. Adapted with permission from ref. 36. Copyright©, 2017, American Chemical Society.

low DASA concentrations on the mesophase level, DASA photoswitching was found to be irreversible in the liquid crystalline system (Figure 1.22c). The authors hypothesize that the structural change stems from both the change in structure upon photoswitching (irreversible) and potential local photothermal effects (reversible). Once cyclized, DASA **35** could transition into the water layer, thus stabilizing the cyclized form.

1.4.5 Wavelength-selective photoswitching

The spectra of DASAs show – in most cases – an optical window with no significant absorption bands between 300 nm and 450 nm (Figure 1.23a). In this spectral region, other photochromes with compatible absorption spectra can be operated. This complementarity allows for wavelength-selective addressing of photochromes. This concept is well-known and frequently employed for photo-removable protecting groups,²⁴ but until recently it has not been extended in an orthogonal fashion to photoswitches. In 2016, our group showed that the combination of azobenzenes (**36–39**) and DASAs (**1** or **12**) allows orthogonal photo-control in toluene (Figure 1.23b, see also Chapter 2).²³ Even though the combination of photoswitches to molecular dyads or triads is well-known in the field of molecular logics, such studies most often focus on properties that emerge from energetic coupling of two chromophores.^{37,38} To test to what extent such coupling would be observed in one molecule, an azobenzene and DASA were connected through alkyl linkers differing in length (compounds **40** and **41**; Figure 1.24a). Indeed, some coupling was observed: especially when addressing the DASA moiety, a *cis-trans* isomerization of the azobenzene moiety was induced (Figure 1.24a, *i*) irradiation 3 and *ii*) irradiation 3 and 4).

This combination was then used as a molecular machine using an azobenzene to control binding to α -cyclodextrin, while the DASA moiety can control phase-transfer between an organic phase (toluene) and an aqueous phase (Figure 1.24b).

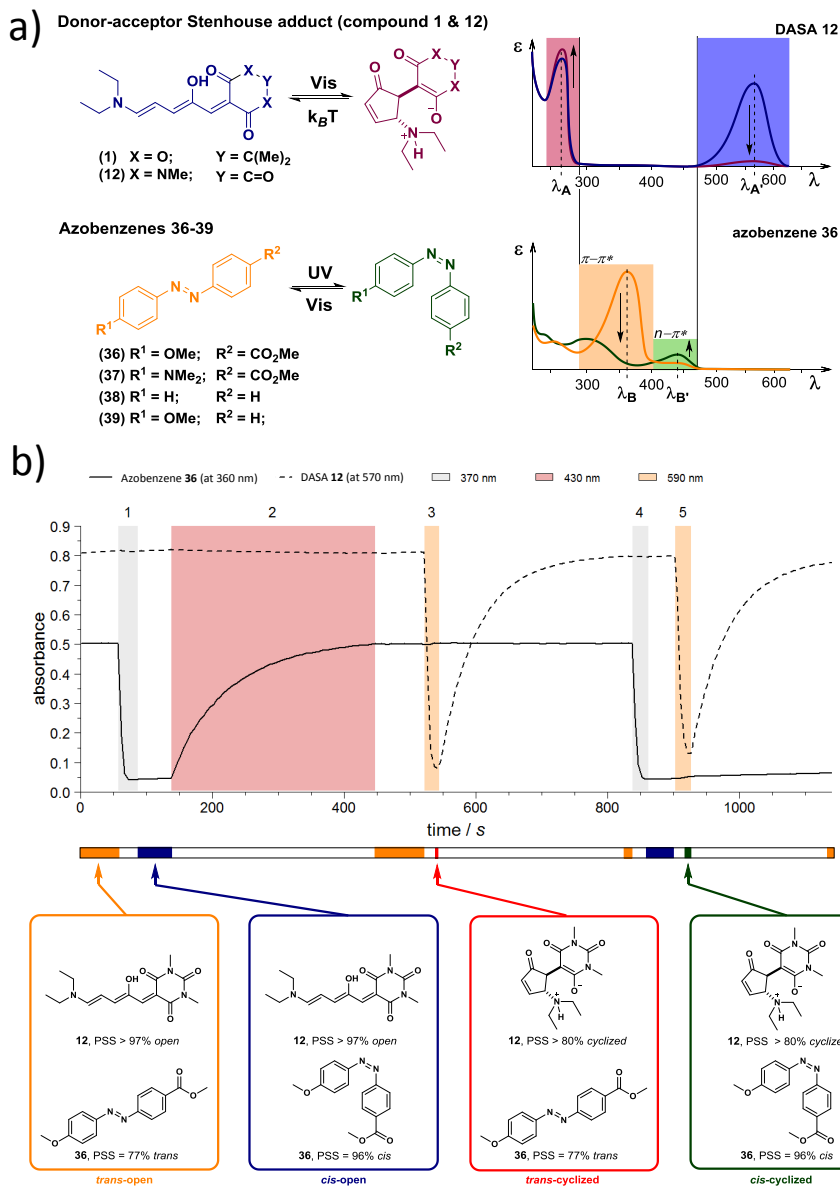


Figure 1.23 | Orthogonal photoswitching of a combination of donor–acceptor Stenhouse adducts and azobenzenes: a) principle and spectral compatibility; b) proof of principle of orthogonal photoswitching of **36** and **12** in toluene. Adapted with permission from ref. 23. Copyright©, 2016, Macmillan Publishers Limited, part of Springer Nature.

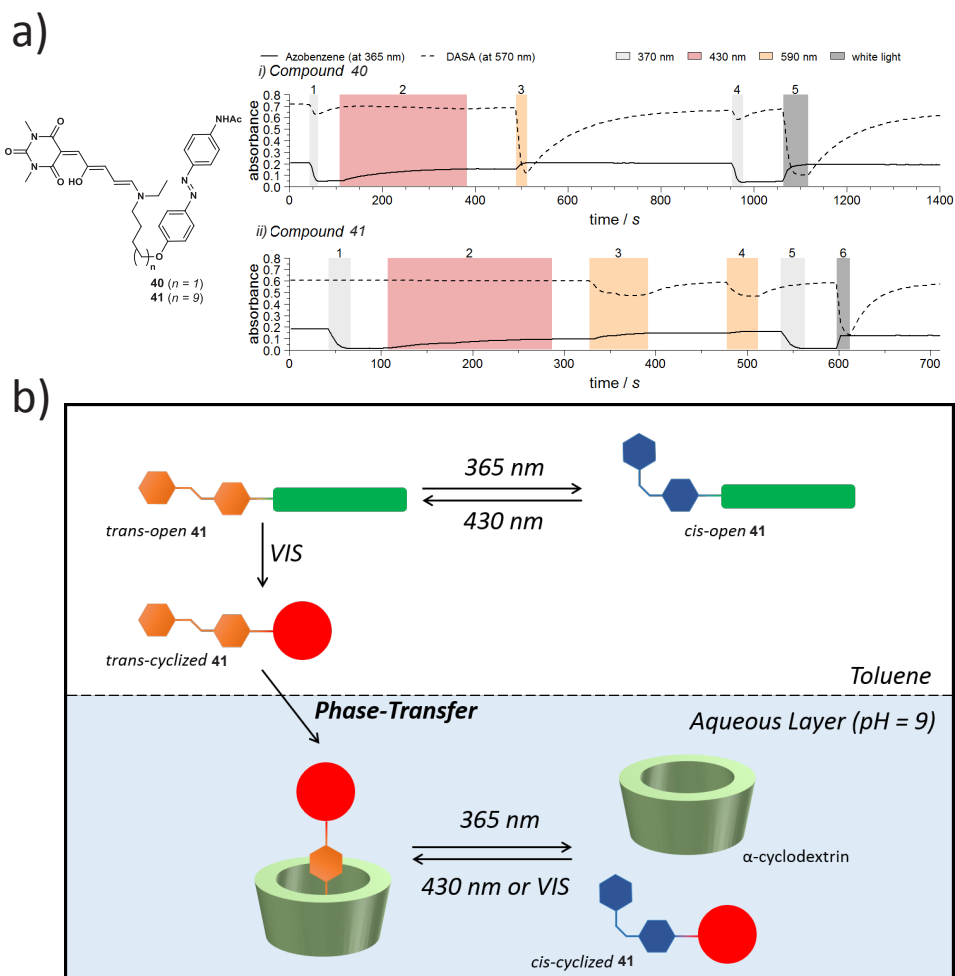


Figure 1.24 | Molecular machine making use of a dyad of an azobenzene and a first-generation DASA: a) intramolecular combination with different linker lengths gives rise to compounds **40** and **41**; b) photoswitching of the DASA moiety of compound **41** leads to light-mediated phase transfer from toluene to the aqueous layer (pH 9), whereas photoswitching of the azobenzene controls reversible host-guest binding to α -cyclodextrin. Adapted with permission from ref. 23. Copyright[©], 2016, Macmillan Publishers Limited, part of Springer Nature.

The potential of a DASA-azobenzene dyad was further studied by Deng, Liu and co-workers (Figure 1.25).³⁹ Compound **42** was synthesized in four steps employing a non-red shifted azobenzene and a Meldrum's acid based DASA. Interestingly, irradiation with 525 nm on *cis-azo-open*-DASA resulted in ring-closure of the DASA as expected, but the *cis*-azobenzene moiety remained unaffected (Figure 1.25a). Furthermore, fluorescence emission spectra

(from exciting the DASA moiety) were reported. Upon photoswitching of the azobenzene moiety with 365 nm within the dyad, a small blue-shift and decrease of the fluorescence emission was observed (Figure 1.25b).

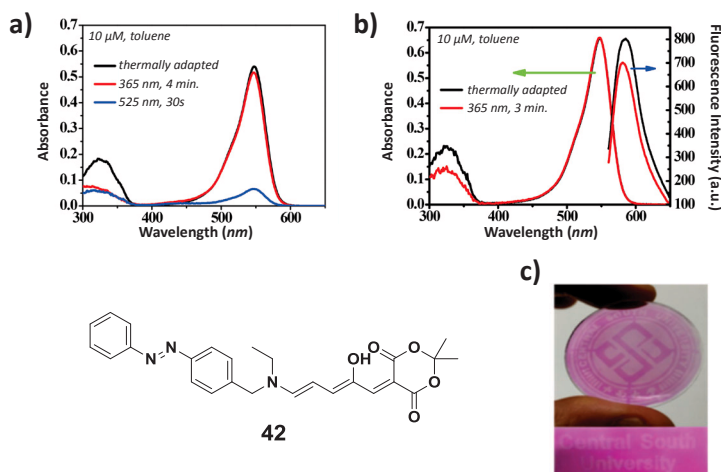


Figure 1.25 | Photoswitching of a molecular dyad: a) absorption spectra of **42** upon application of different light-stimuli in toluene (10 μM); b) absorption and fluorescence emission spectra in toluene; c) photopatterning of **42** dispersed in a polystyrene polymer. Adapted with permission from ref. 39. Copyright[©], 2017, Royal Society of Chemistry.

Deng, Liu and co-workers also used the DASA-azobenzene combination **42** for molecular logical units, specifically the NOR- and the INHIBIT-gate.³⁹ Furthermore, when immersed in a polystyrene-based thin film, photopatterning (Figure 1.25c) was achieved under visible light irradiation. Similar to what was observed by the groups of Hooper and Read de Alaniz,³⁰ the device showed thermally reversible photoswitching.

Read de Alaniz and co-workers showed that wavelength selective photoswitching was also possible with two second-generation DASAs.¹⁴ Within their tunable spectral range of absorption, a pair of second-generation DASAs **14** and **43** can be found, which have regions of non-overlap that allows for selective photoswitching (Figure 1.26a). Importantly, wavelength-selective photoswitching was also possible for DASAs suspended in drop-cast poly(methyl methacrylate) (PMMA) polymer films (Figure 1.26b), where reversible photoswitching is possible and promoted by heating of the cyclized form.

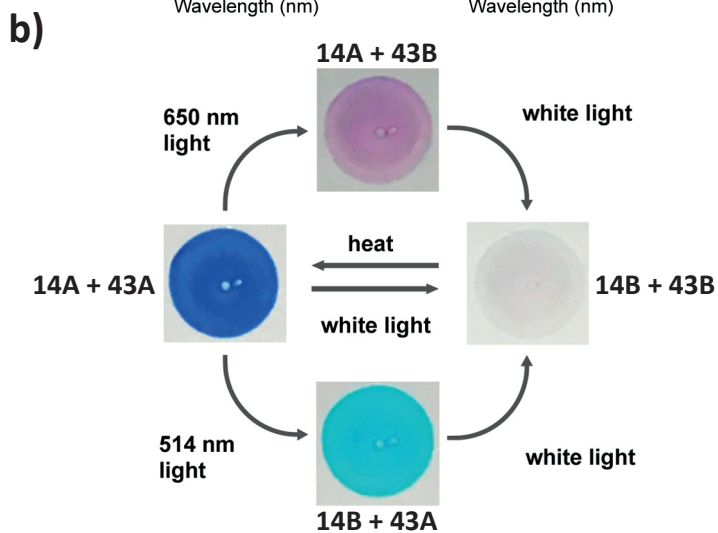
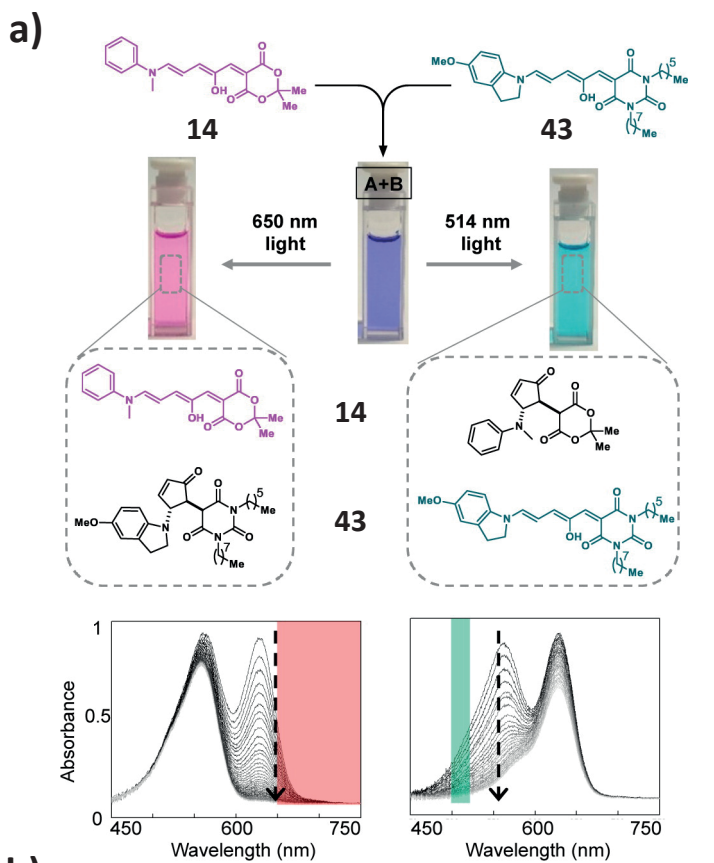


Figure 1.26 | Wavelength selective photoswitching of a combination of second-generation DASAs in solution and as a suspension in a polymer: a) combination of **14** and **43** in solution and their absorption spectra upon selective photoswitching; b) compounds **14** and **43** (~1 wt%) suspended in PMMA drop cast polymer films. Adapted with permission from ref. 14. Copyright®, 2016, American Chemical Society.

Wavelength-selective photoswitching is also possible for covalently attached DASAs in poly(methyl acrylate) (PMA) polymers (*vide supra*, Figure 1.21).³⁵ Here, tertiary photopatterning with high spatial resolution (Figure 1.27) was achieved. Notably, photoswitching was non-orthogonal, but good enough for patterning purposes.

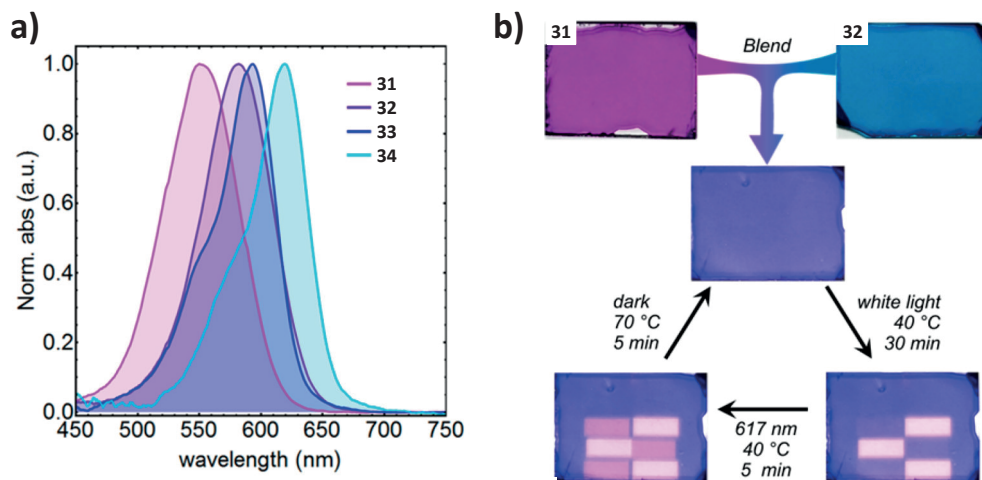


Figure 1.27 | Wavelength-selective photoswitching of secondary DASAs in PMA polymers: a) normalized absorption spectra of compounds **31**–**34**; b) tertiary photopatterning using different wavelength of irradiation. Adapted with permission from ref. 35. Copyright®, 2017, American Chemical Society.

Initial investigations towards wavelength selective photoswitching are promising. When combining photoswitches, the thermal stability of the isomers plays a crucial role. T-type photoswitches are easier to combine than P-type photoswitches, as the thermal back-reaction in the case of T-type photoswitches renders the need for a further wavelength of irradiation for control unnecessary. The combination of azobenzenes and DASAs thus relies on three selective wavelengths of irradiation and a thermal process, whereas the combination of two DASAs makes use of two irradiation wavelengths and two thermal processes. Future, ideal systems would make use of four distinct wavelengths of irradiations in an orthogonal manner. However, this is difficult: photoswitches normally are not only exhibiting a single absorption band, but show non-negligible absorption through-out the spectrum. Despite being T-type photoswitches, DASAs exhibit very little absorption between 300 and 450 nm allowing combinations with other switches or even photo-labile protecting groups. This does

not mean, however, that other photoswitch combinations will not allow for wavelength-selective photoswitching. If electronic properties of photoswitches are carefully chosen, suitable pairs within the same class or across classes may be found and successfully exploited. While orthogonal control relies on full compatibility of photoswitches, “suboptimal” combinations may benefit from difference in photoswitching kinetics and/or quantum yields. For wavelength-selective uncaging, sequential activation/removal of protecting groups has proven very successful.²⁴ When comparing potential candidates for photoswitch combinations, spiropyrans/spirooxazines are highly interesting for wavelength-selective photoswitching, because of a roughly similar visible light absorption as compared to DASAs in some cases.⁴⁰ Stilbenes, hemithioindigo photoswitches and acyl hydrazones may be used as the component that absorbs in the 300–450 nm optical window where DASAs and some spiropyrans/spirooxazines do not absorb significantly.

1.4.6 Chemosensing

DASAs show responsiveness to stimuli other than light, which renders them suitable as chemosensors.⁴¹ Applications include the detection of nerve gas mimics,⁴² amines,¹⁹ pH and metal ions^{43,44} and the use of this responsiveness in polymer dots⁴³ and molecular logics.⁴⁴

For detecting diethyl cyanophosphate (DCNP, **44**, Figure 1.28), a mimic of Tabun (a chemical warfare agent), Lee and Balamurugan made use of the irreversible covalent modification of the amine donor of DASA **45**.⁴² DCNP activates the amine-donor side-chain based on 2-(2-aminoethoxy)ethanol for cyclization. The resulting quaternary amine breaks conjugation and prevents photo-cyclization.

DASA-photoswitches were incorporated into a polymer obtained by RAFT polymerization of glycidyl methacrylate (GMA) and dimethylacrylamide (DMA). 2-(2-aminoethoxy)ethanol was reacted with the epoxide to provide a secondary amine that then could be used as an attachment point for the DASA photoswitch (resulting in about 6% modification of the polymer with DASAs). Photobleaching of the DASA sidechains in a 1,4-dioxane solution proved irreversible, but upon drying, re-dissolving the polymer in chloroform and warming (40 °C), around 75% of the initial absorbance was reconstituted. The nucleophilic hydroxy group stemming from 2-(2-aminoethoxy)ethanol can attack the electrophilic organophosphorus compound DCNP. Such activation allows nucleophilic attack by the amine donor to cyclize to form a quaternary morpholino group (Figure 1.28a), which leads to discoloration of the polymer by breaking conjugation. The dose-dependent discoloration of DASA was used for sensing applications both in solution (as polymer) and gas phase (as spin-coated polymer, Figure 1.28b). Once reacted, the switch cannot cyclize anymore.

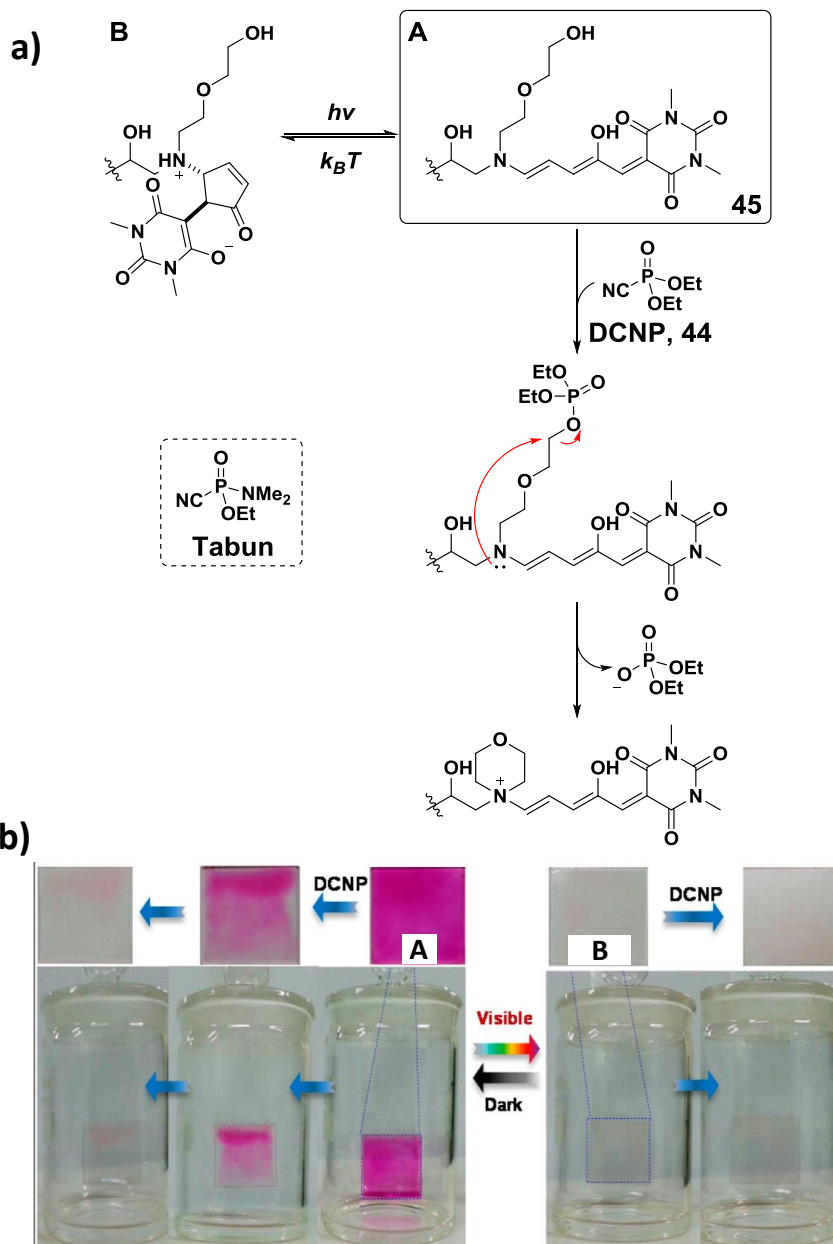


Figure 1.28 | Sensing of diethyl cyanophosphate (DCNP, **44**): a) irreversible modification of the donor-amine by DCNP-induced side-chain cyclization. Photoswitching relies on the integrity of the amine donor; b) light-controlled gas-phase detection of DCNP vapor. Adapted with permission from ref. 42. Copyright ©, 2016, American Chemical Society.

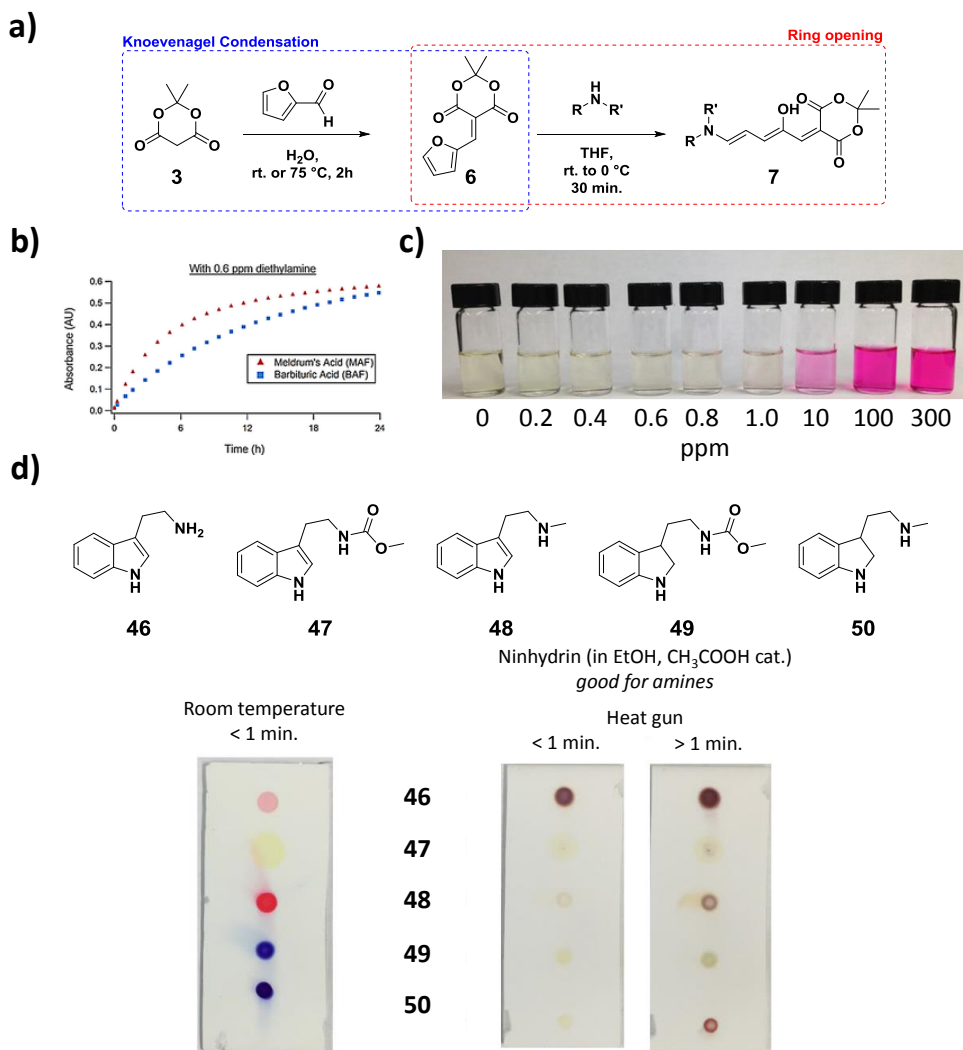


Figure 1.29 | Chemosensing of amines by utilizing the DASA synthetic route: a) DASA synthesis; b) comparison of acceptors with respect to their response to diethylamine (monitored in THF at 532 nm); c) colorimetric detection of the reaction of **6** (20 mM in THF) and diethylamine after 5 min. at different concentrations (in ppm); d) thin-layer chromatography stain developed from this method and compared to ninhydrin staining show-cased on compounds **46–50**. Adapted with permission from ref. 19. Copyright[©], 2017, Wiley-VCH Verlag GmbH & Co. KGaA.

Another approach to chemosensing to detect primary and secondary amines¹⁹ (Figure 1.29) by Read de Alaniz, Hawker and co-workers made use of the synthetic route to DASAs involving

a ring-opening of the activated furan with a secondary amine (*vide supra*).^{12,13} Compound **6** (Meldrum's activated furan, MAF; Figure 1.29a) is yellow, but immediately turns strongly purple/reddish ($\epsilon(\lambda_{\text{max}}) \sim 10^5 \text{ M}^{-1} \text{ cm}^{-1}$) upon addition of the amine forming DASA **1**. Detection of amines was successful on solid support, in solution and gas phase down to sub-ppm level.

Furan rings activated with Meldrum's acid open about two times faster upon addition of diethylamine, as compared to 1,3-dimethyl barbituric acid derivatives (Figure 1.29b). The formation of the DASA product results in a strong color change allowing for a colorimetric read-out (Figure 1.29c). The nature of the amine nucleophile is crucial, with secondary > primary > ammonia (fastest to slowest) allowing to distinguish different types of amines. Other nucleophiles (O-, S- and P-based) showed no or very slow reaction with the activated furans. Nylon filter membranes soaked in THF solutions of compound **6** and dried were able to reliably detect amine vapor at low concentrations. This allowed for instance sensing of volatile amines from the decay of two fish samples (cod and tilapia) over the course several days. Worth highlighting is certainly a Thin-layer chromatography stain based on this reaction (20 mM **6** solution in THF) that allows easy and practical staining of different types of amines (**46–50**, Figure 1.29d). The easily prepared solution is bench-top stable (over six months) and thus presents a procedure that is certainly commendable for organic synthesis laboratories.

DASAs can also be used for the chemosensing of Cu^{2+} and Fe^{3+} ions.⁴³ Wang and co-workers utilized DASA-functionalized polymer dots that respond both to light and change in pH (Figure 1.30a) and that can detect metal ions. Functionalization of branched polyethyleneimine ($M_w = 600 \text{ g/mol}$) with compound **6** in ethanol lead to the formation of DASA-modified polymer dots (Figure 1.30b) with an absorption maximum at 366 nm ($n-\pi^*$ and surface moieties of polymer dots) and 522 nm (DASA absorption) in ethanol. These dots exhibit an interesting change of fluorescence emission spectra upon changing the excitation wavelength (Figure 1.30c). Fluorescence also allows for the detection of Cu^{2+} and Fe^{3+} ions, as increasing concentrations result in a net-decrease of fluorescence. Detection limits were determined to 10.1 nM (Fe^{3+}) and 1.3 nM (Cu^{2+}).

Besides chemosensing, Wang and co-workers studied the behavior of DASA **1** in acidic or basic ethanol (pH 6 or pH 8, respectively, Figure 1.30d). Basifying resulted in a blue-shift of the absorption spectrum and cyclization. Despite the fact that acid stabilizes the open form, reversible pH-dependent switching was not possible. DASA-functionalized polymer dots, however, showed reversible switching upon alternating the pH. Light-irradiation caused irreversible cyclization, but in acidic environment ring-opening was observed. Upon placing in water, DASAs cyclized rapidly and spontaneously. Table 1.4 summarizes size-changes of the polymer dots under different conditions (both measured with TEM and dynamic light scattering, DLS).⁴³ These changes can be attributed to different aggregation states: cyclization reduces the size and changes polarity of the DASA moiety which results in dissociation of the particles. Reducing pH can lead to a swelling of the dots due to repulsion of the positively charged amine groups. Changes in aggregation, size and solubility would also influence fluorescence.

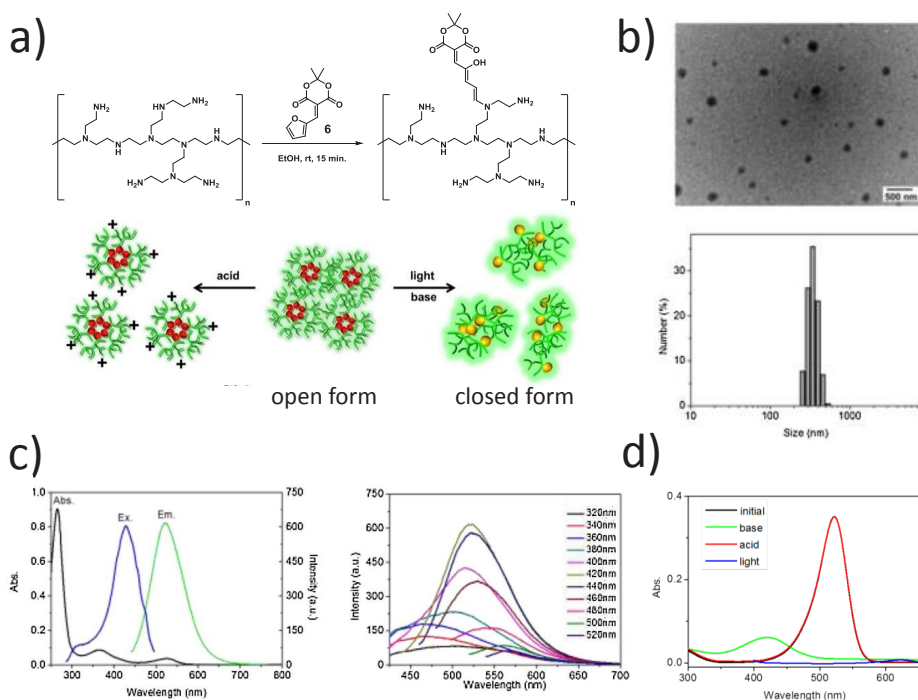


Figure 1.30 | Stimuli-responsive polymer dots: a) polymer dot synthesis; b) TEM and size-distribution of polymer dots in ethanol (DLS analysis); c) UV/vis absorption spectrum, excitation spectrum (Ex., $\lambda_{\text{em}} = 520 \text{ nm}$) and emission spectrum (Em., $\lambda_{\text{ex}} = 420 \text{ nm}$) and fluorescence emission spectra depending on the excitation wavelength in ethanol; d) comparison of absorption spectra of DASA 1 in ethanol at pH 6 and pH 8 and under irradiation. Adapted with permission from ref. 43. Copyright[®], 2017, ScienceDirect, Elsevier.

Table 1.4 | Polymer dot sizes (in nm) as estimated by TEM and dynamic light scattering (DLS) under different conditions. Data taken from ref. 43.

Method	Ethanol	Ethanol (pH 8)	Ethanol (pH 6)	Ethanol (irr.)	Water
TEM	150	6	60	70	65
DLS	342	122	50	164	200

Another group reported on the detection of Cu^{2+} concentrations based on DASA fluorescence modulation in solution.⁴⁴ Taking the well-known 1,8-naphthalimide fluorescent moiety and connecting it to a second-generation DASA gives rise to adduct **51** (Figure 1.31a). Two absorption bands dominate the spectrum in chloroform (Figure 1.31b): one at 440 nm corresponding to the 1,8-naphthalimide moiety and one corresponding to the DASA photoswitch at 625 nm. The fluorescence spectrum shows two bands upon excitation with 442 nm light, corresponding to the open form (620 – 720 nm, $\phi_{\text{ex}}^{\text{open}} = 0.23$) and the closed form (520 – 620 nm, $\phi_{\text{ex}}^{\text{closed}} = 0.46$), both present in equilibrium in chloroform (Figure 1.31b). The fluorescence emission of the closed form overlaps with the DASA absorption band (open form) thus effectively reducing the fluorescence by energy transfer. Cyclization of the DASA moiety with white light result in a net-increase of fluorescence intensity (Figure 1.31b). In chloroform, the observed equilibrium between the open and closed form amounts to 22:78 (as compared to the corresponding indoline-based DASA: 31:69 in deuterated dichloromethane¹⁴). In acetonitrile, fluorescence is dramatically reduced. Addition of trifluoroacetic acid leads to a decrease of both the absorption and fluorescence and prevents photobleaching, which is attributed to protonation of the indoline moiety and thus breaking of the conjugation (Figure 1.31b). Addition of copper(II) acetate reduces absorption and fluorescence intensity of the open form, but due to reduced coordination in the cyclized form, a fluorescence increase is observed upon photoswitching (Figure 1.31b). Luo and Qu and co-workers⁴⁴ make use of these properties and showcase the potential of compound **51** as NOR and AND logical gate (Figure 1.31c). The compound itself is relatively fatigue resistant showing about 5% fatigue over ten photoswitching cycles.

Within three years since the introduction of donor–acceptor Stenhouse adducts, not only have the switching properties been better understood^{20–22,26,45} and further optimized,^{14,15} but also the field has seen a remarkable number of applications. Successful examples range from chemical sensing, to applications in material science and surface chemistry and drug-delivery. Notably, DASAs can be combined with azobenzenes to form a complementary pair for orthogonal control of function, a concept that hopefully will be extended to other photoswitch combinations, for example spiropyrans/spirooxazines, diarylethenes, hemithioindigo photoswitches and fulgides/fulgimides. Many of the described applications make deliberate use of DASA properties that are immediate consequences of the photoswitching mechanism. With a better understanding of it, the field is eagerly awaiting further improvements and exciting applications in new avenues.

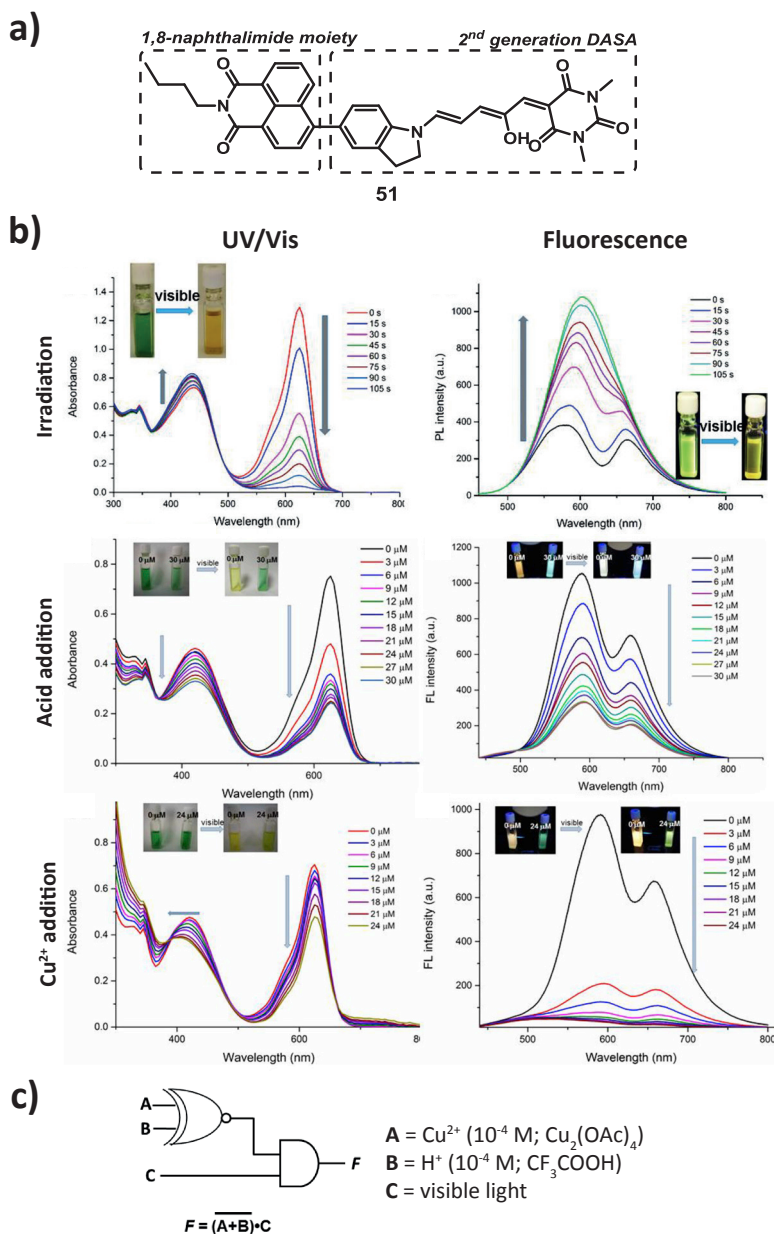


Figure 1.31 | Fluorescent DASA adduct shows fluorescence modulation for different stimuli (white light, acid and Cu²⁺): a) compound **51**; b) UV/vis and fluorescence spectra and their response to irradiation, addition of acid or copper(II) acetate in chloroform; c) molecular logic gate constructed from this system. Adapted with permission from ref. 44. Copyright©, 2017, ScienceDirect, Elsevier.

1.5 Stenhouse Photoswitches

Read de Alaniz and co-workers described the previous work that led to the discovery of DASA photoswitches.^{12,13} The following section, however, aims at providing a brief discussion of the much older Stenhouse salts and their chemistry to highlight similarities and differences to DASAs (Figures 1.32 and 1.33). Together, DASAs and Stenhouse salts form the structural class of Stenhouse photoswitches. While DASAs make use of a cyclic bis-carbonyl-based acceptor that allows for efficient hydrogen bonding to the C₂-hydroxy group, Stenhouse salts use an iminium ion as the acceptor and are thus inherently charged and lack a hydrogen-bond (Figure 1.32). Their photochemistry remains to be explored.

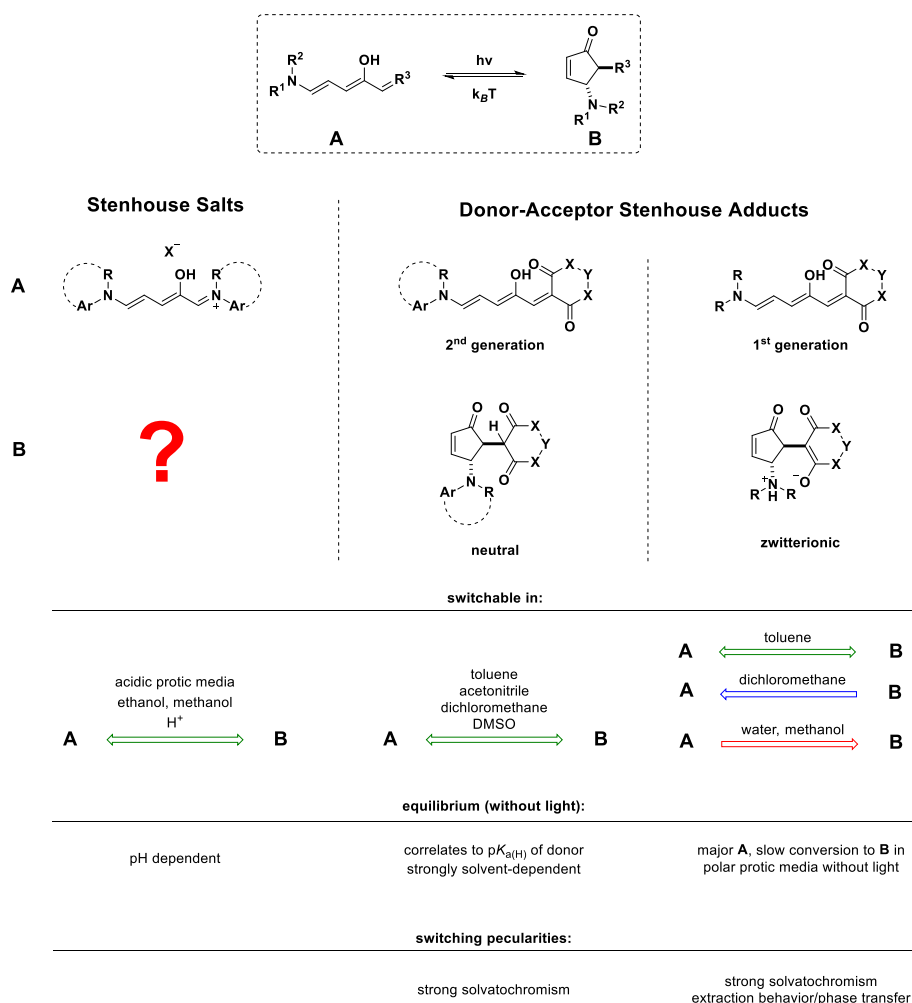


Figure 1.32 | Structure of Stenhouse photoswitches and comparison of their properties.

Although much older – Stenhouse salts were first described in the middle of the 19th century by the Scottish chemist John Stenhouse (see opening quote)¹⁸ – their ability to photoswitch was not discovered until 1982.⁴⁶ Honda's work still remains the only report of their photoswitching and gives initial insights into the importance of pH and pK_a on their photoswitching behavior. Remarkably, Stenhouse salts have been intimately intertwined with organic chemistry as a developing field: around the turn of the 19th century until deep into the 20th century, an extended discussion was focussed on their chemical structure (Figure 1.33).⁴⁷ Zincke and Mühlhausen proposed an elongated structure, as opposed to a branched structure put forward by Schiff.⁴⁸ Research related to this brought us not only the categorization of polymethine dyes by Walter König, and the Zincke reaction, but also the term Schiff-base (imine) by Hugo Schiff.

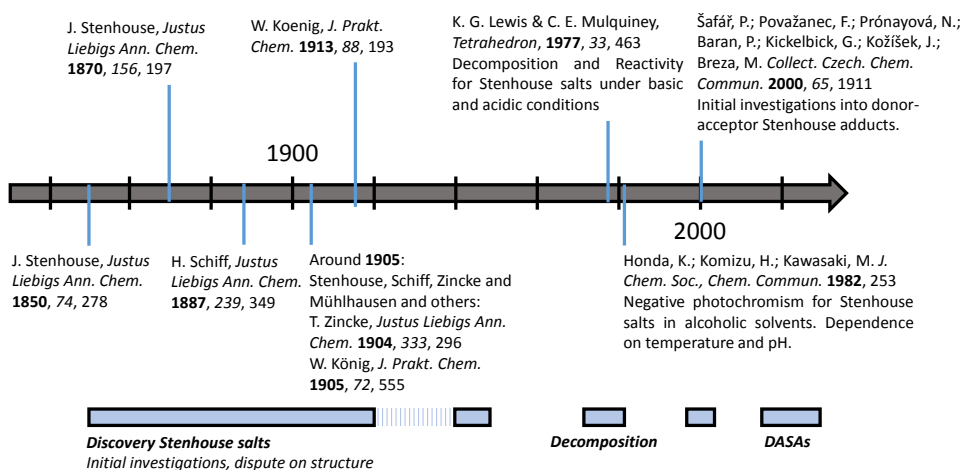


Figure 1.33 | Brief historical overview of the development of Stenhouse switches.

With their photoswitching properties largely unexplored, Stenhouse salts offer an interesting venue for novel applications that could complement DASAs.

1.6 Acknowledgments

We would like to thank Prof. Dr W. R. Browne, Dr S. J. Wezenberg and Kaja Sitkowska (University of Groningen, The Netherlands), Prof. Dr W. J. Buma (University of Amsterdam, The Netherlands), Prof. Dr Claudia Filippi (University of Twente, The Netherlands), Prof. Dr P. Foggi, Dr L. Bussotti, Dr M. Di Donato, Dr A. Iagatti and Dr A. Lapini (LENS, Italy), Prof. Dr D. Jacquemin, Dr A. D. Laurent (Université de Nantes, France), Prof. Dr M. Medved' (Palacký University in Olomouc, Czech Republic/Matej Bel University, Slovak Republic) and Prof. Dr J. Read de Alaniz (UC Santa Barbara, USA) for fruitful discussions. Further, we thank the Netherlands Organization for Scientific Research (NWO–CW, TOP grant to B.L.F., VIDI grant no. 723.014.001 for W.S.), the Royal Netherlands Academy of Arts and Sciences Science

(KNAW), the Ministry of Education, Culture and Science (Gravitation program 024.001.035), and the European Research Council (Advanced Investigator Grant, no. 227897 to B.L.F.) for financial support. M.M.L. thanks the Swiss Study Foundation for a fellowship.

1.7 References

1. *Molecular Switches*, 2nd ed.; Feringa, B. L., Browne, W. R., Eds.; Wiley-VCH: Weinheim, Germany, **2011**.
2. Bouas-Laurent, H.; Dürr, H. *Pure Appl. Chem.* **2001**, *73* (4), 639–665.
3. Briekke, C.; Rohrbach, F.; Gottschalk, A.; Mayer, G.; Heckel, A. *Angew. Chem. Int. Ed.* **2012**, *51* (34), 8446–8476.
4. Klán, P.; Šolomek, T.; Bochet, C. G.; Blanc, A.; Givens, R.; Rubina, M.; Popik, V.; Kostikov, A.; Wirz, J. *Chem. Rev.* **2013**, *113* (1), 119–191.
5. Velema, W. A.; Szymański, W.; Feringa, B. L. *J. Am. Chem. Soc.* **2014**, *136* (6), 2178–2191.
6. Broichhagen, J.; Frank, J. A.; Trauner, D. *Acc. Chem. Res.* **2015**, *48* (7), 1947–1960.
7. Lerch, M. M.; Hansen, M. J.; van Dam, G. M.; Szymanski, W.; Feringa, B. L. *Angew. Chem. Int. Ed.* **2016**, *55* (37), 10978–10999.
8. Stolik, S.; Delgado, J. A.; Pérez, A.; Anasagasti, L. *J. Photochem. Photobiol. B Biol.* **2000**, *57* (2–3), 90–93.
9. Dong, M.; Babalhavaej, A.; Samanta, S.; Beharry, A. A.; Woolley, G. A. *Acc. Chem. Res.* **2015**, *48* (10), 2662–2670.
10. Bléger, D.; Hecht, S. *Angew. Chem. Int. Ed.* **2015**, *54* (39), 11338–11349.
11. Barachevsky, V. A. *Rev. J. Chem.* **2017**, *7* (3), 334–371.
12. Helmy, S.; Leibfarth, F. A.; Oh, S.; Poelma, J. E.; Hawker, C. J.; Read de Alaniz, J. *J. Am. Chem. Soc.* **2014**, *136* (23), 8169–8172.
13. Helmy, S.; Oh, S.; Leibfarth, F. A.; Hawker, C. J.; Read de Alaniz, J. *J. Org. Chem.* **2014**, *79* (23), 11316–11329.
14. Hemmer, J. R.; Poelma, S. O.; Treat, N.; Page, Z. A.; Dolinski, N. D.; Diaz, Y. J.; Tomlinson, W.; Clark, K. D.; Hooper, J. P.; Hawker, C.; *et al.* *J. Am. Chem. Soc.* **2016**, *138* (42), 13960–13966.
15. Mallo, N.; Brown, P. T.; Iranmanesh, H.; MacDonald, T. S. C.; Teusner, M. J.; Harper, J. B.; Ball, G. E.; Beves, J. E. *Chem. Commun.* **2016**, *52* (93), 13576–13579.
16. Nieto Faza, O.; Silva López, C.; Álvarez, R.; De Lera, Á. R. *Chem. - Eur. J.* **2004**, *10* (17), 4324–4333.
17. Piutti, C.; Quartieri, F. *Molecules* **2013**, *18* (10), 12290–12312.
18. Stenhouse, J. *Justus Liebigs Ann. Chem.* **1850**, *74* (3), 278–297.
19. Diaz, Y. J.; Page, Z. A.; Knight, A. S.; Treat, N. J.; Hemmer, J. R.; Hawker, C. J.; Read de Alaniz, J. *Chem. Eur. J.* **2017**, *23* (15), 3562–3566.
20. Lerch, M. M.; Wezenberg, S. J.; Szymański, W.; Feringa, B. L. *J. Am. Chem. Soc.* **2016**, *138* (20), 6344–6347.
21. Di Donato, M.; Lerch, M. M.; Lapini, A.; Laurent, A. D.; Iagatti, A.; Bussotti, L.; Ihrig, S. P.; Medved', M.; Jacquemin, D.; Szymański, W.; Buma, W. J.; Foggi, P.; Feringa, B. L. *J. Am. Chem. Soc.* **2017**, *139* (44), 15596–15599.
22. Lerch, M. M.; Medved', M.; Lapini, A.; Laurent, A. D.; Iagatti, A.; Bussotti, L.; Szymański, W.; Buma, W. J.; Foggi, P.; Di Donato, M.; Feringa, B. L. *J. Phys. Chem. A* **2018**, *122* (4), 955–964.
23. Lerch, M. M.; Hansen, M. J.; Velema, W. A.; Szymański, W.; Feringa, B. L. *Nat. Commun.* **2016**, *7*, 12054.
24. Hansen, M. J.; Velema, W. A.; Lerch, M. M.; Szymański, W.; Feringa, B. L. *Chem. Soc. Rev.* **2015**, *44* (11), 3358–3377.
25. König, W. J. *für Prakt. Chemie* **1926**, *112* (1), 1–36.
26. Laurent, A. D.; Medved', M.; Jacquemin, D. *ChemPhysChem* **2016**, *17* (12), 1846–1851.
27. Ahrens, J.; Bian, T.; Vexler, T.; Klajn, R.

- ChemPhotoChem* **2017**, *1* (5), 230–236.
28. Blake, A. J.; McNab, H.; Monahan, L. C. *J. Chem. Soc. Perkin Trans. 2* **1991**, *2* (0), 2003–2010.
29. Riveira, M. J.; Marsili, L. A.; Mischne, M. P. *Org. Biomol. Chem.* **2017**, *15*, 9255–9274.
30. Mason, B. P.; Whittaker, M.; Hemmer, J.; Arora, S.; Harper, A.; Alnemrat, S.; McEachen, A.; Helmy, S.; Read De Alaniz, J.; Hooper, J. P. *Appl. Phys. Lett.* **2016**, *108* (4), 41906.
31. Helmy, S.; Read de Alaniz, J. *Adv. Heterocycl. Chem.* **2015**, *117*, 131–177.
32. Poelma, S. O.; Oh, S. S.; Helmy, S.; Knight, A. S.; Burnett, G. L.; Soh, H. T.; Hawker, C. J.; Read de Alaniz, J. *Chem. Commun.* **2016**, *52* (69), 10525–10528.
33. Singh, S.; Friedel, K.; Himmerlich, M.; Lei, Y.; Schlingloff, G.; Schober, A. *ACS Macro Lett.* **2015**, *4* (11), 1273–1277.
34. Sinawang, G.; Wu, B.; Wang, J.; Li, S.; He, Y. *Macromol. Chem. Phys.* **2016**, *217* (21), 2409–2414.
35. Ulrich, S.; Hemmer, J. R.; Page, Z. A.; Dolinski, N. D.; Rifaie-Graham, O.; Bruns, N.; Hawker, C. J.; Boesel, L. F.; Read De Alaniz, J. *ACS Macro Lett.* **2017**, *6* (7), 738–742.
36. Jia, S.; Du, J. D.; Hawley, A.; Fong, W.-K.; Graham, B.; Boyd, B. J. *Langmuir* **2017**, *33* (9), 2215–2221.
37. de Silva, A. P. *Molecular Logic-Based Computation, Monographs in Supramolecular Chemistry*; RSC Publishing, 2012.
38. Fihey, A.; Perrier, A.; Browne, W. R.; Jacquemin, D. *Chem. Soc. Rev.* **2015**, *44* (11), 3719–3759.
39. Tang, F.-Y.; Hou, J.-N.; Liang, K.-X.; Liu, Y.; Deng, L.; Liu, Y.-N. *New J. Chem.* **2017**, *41* (14), 6071–6075.
40. Minkin, V. I. *Chem. Rev.* **2004**, *104* (5), 2751–2776.
41. *Chemosensors: Principles, Strategies, and Applications*; Wang, B., Anslyn, E. V., Eds.; Wiley-VCH: Hoboken, N.J., 2011.
42. Balamurugan, A.; Lee, H. A. *Macromolecules* **2016**, *49* (7), 2568–2574.
43. Zhong, D.; Cao, Z.; Wu, B.; Zhang, Q.; Wang, G. *Sens. Actuators, B* **2018**, *254*, 385–392.
44. Yang, S.; Liu, J.; Cao, Z.; Li, M.; Luo, Q.; Qu, D. *Dye. Pigm.* **2018**, *148*, 341–347.
45. Belhboub, A.; Boucher, F.; Jacquemin, D. *J. Mater. Chem. C* **2017**, *5* (7), 1624–1631.
46. Honda, K.; Komizu, H.; Kawasaki, M. *J. Chem. Soc. Chem. Commun.* **1982**, *0* (4), 253–254.
47. Lewis, K. G.; Mulquiney, C. E. *Tetrahedron* **1977**, *33* (5), 463–475.
48. Schiff, H. *Justus Liebigs Ann. Chem.* **1887**, *239* (3), 349–385.

